NASA TECHNICAL MEMORANDUM

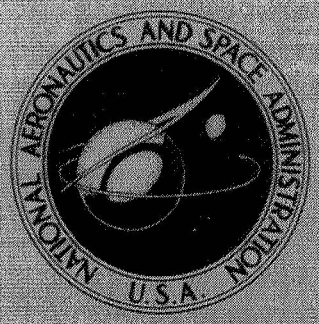

NASA TM X-2265

NASA TM X-2265

AERODYNAMIC CHARACTERISTICS OF A BOOSTER AND AN ASCENT SHUTTLE CONFIGURATION FROM MACH 0.28 TO MACH 10.4

by Peter T. Bernot and Jarrett K. Huffman

Langley Research Center
Hampton, Va. 23365

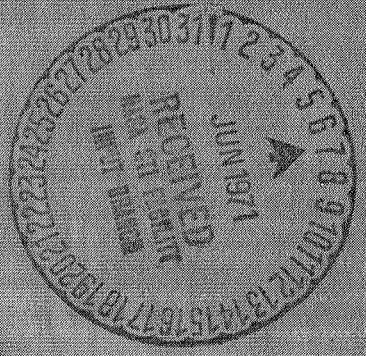

NATIONAL AERONAUTICS AND SPACE ADMINISTRATION • WASHINGTON, D. C. • MAY 1971

1. Report No.	2. Government Accession No.	3. Recipient's Catalog No.
NASA TM X-2265		

4. Title and Subtitle	5. Report Date
AERODYNAMIC CHARACTERISTICS OF A BOOSTER AND AN ASCENT SHUTTLE CONFIGURATION FROM MACH 0.28 TO MACH 10.4	May 1971
	6. Performing Organization Code

7. Author(s)	8. Performing Organization Report No.
Peter T. Bernot and Jarrett K. Huffman	L-7628
	10. Work Unit No.
	124-07-24-06

9. Performing Organization Name and Address	11. Contract or Grant No.
NASA Langley Research Center Hampton, Va. 23365	

12. Sponsoring Agency Name and Address	13. Type of Report and Period Covered
National Aeronautics and Space Administration Washington, D.C. 20546	Technical Memorandum
	14. Sponsoring Agency Code

15. Supplementary Notes

16. Abstract

Force tests of a two-stage fully reusable shuttle concept similar to that considered in a recent study reported in Integral Launch and Reentry Vehicle Systems (Rep. MDC E0049) by McDonnell Douglas Astronautics Co. were performed at Langley Research Center over a Mach number range of 0.28 to 10.4. Longitudinal and some lateral-directional aerodynamic characteristics were obtained for the booster and the ascent configuration comprised of the booster and HL-10 orbiter. Also, trimmed characteristics for the booster are presented at subsonic and hypersonic speeds; characteristics of the HL-10 orbiter are well documented elsewhere. An interference-drag parameter for the ascent configuration over the speed range is also presented.

17. Key Words (Suggested by Author(s))	18. Distribution Statement
Shuttle configurations	Unclassified – Unlimited

19. Security Classif. (of this report)	20. Security Classif. (of this page)	21. No. of Pages	22. Price*
Unclassified	Unclassified	62	$3.00

*For sale by the National Technical Information Service, Springfield, Virginia 22151

AERODYNAMIC CHARACTERISTICS OF A BOOSTER AND AN ASCENT SHUTTLE CONFIGURATION FROM MACH 0.28 TO MACH 10.4

By Peter T. Bernot and Jarrett K. Huffman
Langley Research Center

SUMMARY

Longitudinal and lateral-directional aerodynamic characteristics were obtained in wind-tunnel tests on a clipped-delta-wing booster and the ascent configuration comprised of the booster and the HL-10 orbiter.

The results of this investigation indicated that the booster was longitudinally and laterally stable over the planned operational flight regimes and was directionally stable at Mach numbers up to 0.70. At supersonic speeds, directional stability existed only at lower ranges of angle of attack while instability occurred over the entire angle-of-attack range at hypersonic speeds. At low-subsonic speeds, a maximum trim lift-drag ratio of about 7 was obtained at a Reynolds number of 11.4×10^6 based on model length. At Mach 10.4, a maximum trim lift coefficient of 0.63 was measured at an angle of attack near 50^o.

The ascent configuration was longitudinally unstable at Mach 10.4, which is representative of nominal staging velocity. Interference-drag losses for the configuration are highly sensitive to angle of attack and can result in payload reductions up to 4.8 percent for a 15.2-MN (3.4-million-pound) lift-off weight.

INTRODUCTION

In the development of an economical space-transportation system, the two-stage fully reusable concept is being given considerable attention and several configurational approaches are now being studied by industry and government. The purpose of this paper is to present the results of wind-tunnel force tests over a Mach number range of 0.28 to 10.4 of a two-stage system similar to that studied recently for NASA. (See ref. 1.) The booster had a clipped-delta wing and a vertical tail; the HL-10 vehicle was the second stage. For the wind-tunnel investigation, the orbiter length was one-half that of the booster, their bases were alined, and their reference center lines parallel. Longitudinal and lateral-directional aerodynamic data were obtained from balance measurements for the booster and ascent configuration in facilities at the Langley Research Center. Aerodynamic characteristics of the HL-10 orbiter over the Mach number range are thoroughly documented and are not repeated in this paper.

SYMBOLS

Longitudinal aerodynamic data are referred to the stability-axis system while the lateral-directional aerodynamic data are referred to the body-axis system. The moment reference center for the booster alone was located on the model center line at 66 percent of model length from the nose. For the ascent configuration, the moment reference center employed in the subsonic and supersonic tests was located at 45 percent of booster length behind the nose and 2 percent below the booster center line while, for the hypersonic tests, the moment reference was 74.1 percent behind the booster nose and 6.6 percent below the booster center line. These reference centers are representative center-of-gravity locations for the ascent configuration at lift-off and burnout, respectively. Values are given in both SI and U.S. Customary Units. The measurements and calculations were made in U.S. Customary Units.

b	booster wing span
$C_{D'}$	drag coefficient, $\frac{\text{Drag}}{qS}$
C_L	lift coefficient, $\frac{\text{Lift}}{qS}$
C_l	rolling-moment coefficient, $\frac{\text{Rolling moment}}{qSb}$
C_{l_β}	effective-dihedral parameter, $\frac{\Delta C_l}{\Delta\beta}$, per degree
$C_{m,s}$	pitching-moment coefficient, $\frac{\text{Pitching moment}}{qSl}$
C_n	yawing-moment coefficient, $\frac{\text{Yawing moment}}{qSb}$
C_{n_β}	directional stability parameter, $\frac{\Delta C_n}{\Delta\beta}$, per degree
C_p	pressure coefficient
C_Y	side-force coefficient, $\frac{\text{Side force}}{qS}$
C_{Y_β}	side-force parameter, $\frac{\Delta C_Y}{\Delta\beta}$, per degree
K	interference parameter, $\frac{C_{D',\text{ascent}}}{C_{D',\text{booster}} + C_{D',\text{orbiter}}}$

L/D	lift-drag ratio, $\frac{C_L}{C_D}$
l	booster length
M	free-stream Mach number
p_o	stagnation pressure
q	free-stream dynamic pressure
R_l	Reynolds number based on booster length and free-stream conditions
r	radius
S	booster reference planform area
T_o	stagnation temperature
x	axial distance measured from booster nose
z	vertical distance measured from booster center line, positive downward
α	angle of attack, based on booster center line, deg
β	angle of sideslip, deg
δ_e	elevon deflection, deg, positive with trailing edge down

Subscript:

max	maximum

APPARATUS AND METHODS

Models

Drawings and photographs of the test configurations are presented in figures 1 to 3. The booster fuselage cross section (fig. 1) had a flat top and bottom with semicircular sides. This configuration incorporated a low wing having 55° of leading-edge sweep and a clipped delta-wing planform. The airfoil was a modified NACA 4415 section mounted

at 3^{o} incidence so that the flat lower surface of the airfoil was coincident with the fuselage lower surface. The vertical tail employed a 6^{o} wedge section with a blunted leading edge having a 50^{o} sweep angle. Two booster models were constructed, one with a 40.64-cm (16-inch) aluminum fuselage with brass wing and tail and the other with a 25.4-cm (10-inch) all-aluminum fuselage. The 25.4-cm (10-inch) model, used only for high-angle-of-attack tests at hypersonic speeds, was supported by a 30^{o} bent sting. This type of mounting necessitated removal of parts of the vertical tail and fuselage afterbody. (See fig. 3(c).) Geometric characteristics of both booster models are presented in table I.

The ascent configuration (fig. 2) consisted of the larger booster model and a cast aluminum model of the HL-10 orbiter having a length of 20.3 cm (8 inches). The models were mated with their reference center lines parallel and their bases alined. A photograph of the ascent configuration is presented in figure 3(b).

Facilities

The low-subsonic tests were performed in the Langley low-turbulence pressure tunnel which is a variable-pressure, continuous-flow facility. The test section is 0.915 meter (3 feet) wide by 2.29 meters (7.5 feet) high. Mach number can be varied from about 0.1 to 0.4 with a Reynolds number variation of 3.3×10^{6} to 49.2×10^{6} per meter (1×10^{6} to 15×10^{6} per foot) at $M = 0.22$.

Data up to Mach 0.85 were obtained in the Langley high-speed 7- to 10-foot tunnel which is an atmospheric, continuous-flow facility. The test section is 2.01 meters (79 inches) high and 2.92 meters (115 inches) wide with a usable length of about 1.52 meters (60 inches). (See ref. 2.)

Supersonic data were obtained in the Langley Unitary Plan wind tunnel which is a variable-pressure, continuous-flow tunnel. This facility has two test sections measuring 1.22 meters (4 feet) square and 2.14 meters (7 feet) long. The nozzles are of the asymmetric sliding-block type which permit continuous variation of Mach numbers from 1.5 to 2.86 in one test section and from 2.3 to 4.63 in the other. (See ref. 3.)

The high-speed tests of this investigation were conducted in the Langley continuous-flow hypersonic tunnel, which is designed to operate over a pressure range of 1.52 to 15.2 MN/m^{2} (15 to 150 atmospheres) at temperatures up to 1090^{o} K (1960^{o} R). Air is heated by an electrical-resistance multitube heater prior to entry into a water-cooled nozzle which has a 79-cm-square (31-inch-square) test section. Continuous operation is achieved by recirculating the airflow through a series of compressors. Mach number varies from about 10.25 to 10.40 with corresponding Reynolds number range of about 1.6×10^{6} to 7.5×10^{6} per meter (0.50×10^{6} to 2.3×10^{6} per foot). (See ref. 4.) The test conditions are summarized in table II.

Methods

Force and moment data were measured by internal, sting-mounted six-component strain-gage balances connected to remotely controlled strut mechanisms. The mode of operation of these mechanisms was different for each facility. For instance, yaw angles were obtained in the low-turbulence pressure tunnel with a bent sting. The high-angle-of-attack sting of the 7- by 10-foot tunnel used a combination of pitch angle and roll angle to obtain the desired sideslip angle. In the hypersonic tests, the entire balance-strut assembly was mounted on an injection mechanism that permitted model injection into the hot air stream from a cooling chamber located adjacent to the test section. (See ref. 4.) Balance temperatures were continuously monitored with thermocouples; thus, the model could be retracted into the chamber when temperature limits were reached without interruption of tunnel flow.

For those tests in the subsonic and supersonic speed ranges, transition strips were used on the booster model according to the methods described in reference 5. In the subsonic tests, the strips consisted of No. 100 carborundum grains and were located 1.52 cm (0.6 inch) aft of the leading edges of the wing and vertical tail and 2.54 cm (1 inch) aft of the fuselage nose. In the supersonic tests, strips of No. 60 carborundum grains were located 1.02 cm (0.4 inch) behind the leading edges and 3.05 cm (1.2 inch) aft of the nose. Similar locations were also used on the orbiter model. All transition bands had a width of about 0.16 cm (0.063 inch).

Angles of attack and sideslip were calculated accounting for model-sting deflections due to aerodynamic load. Jet-boundary and blockage corrections were applied to the subsonic data by the methods of references 6 and 7. The drag coefficients presented herein are uncorrected for base pressure with the exception of those tests at Mach 10.4 where base drag coefficients were less than 0.0007.

The reference areas and lengths for the large and small boosters are listed in table I. The reference values for the large booster were also used for the ascent configuration.

PRESENTATION OF RESULTS AND DISCUSSION

All wind-tunnel data are summarized in the following figures:

Booster Characteristics

Longitudinal.- The longitudinal stability data for the booster over the Mach number range of 0.28 to 10.4 are presented in figure 4 for a center of gravity at 66 percent of booster length. The booster was longitudinally stable except for angles of attack near $C_{L,max}$ at subsonic speeds and below $(L/D)_{max}$ at M = 10.4. These unstable regimes are of no consequence operationally where high-angle-of-attack entry near $C_{L,max}$ after staging is followed by transition to angle of attack near $(L/D)_{max}$ at lower speeds. Maximum untrimmed L/D values of 1.6 and 7.5 were obtained at M = 10.4 at $R_l = 1.33 \times 10^6$ and M = 0.28 at $R_l = 11.4 \times 10^6$, respectively.

In figure 4(h), Newtonian theory using the method of reference 8 is presented for an elevon deflection of 0^o. Using a $C_{p,max}$ equal to 2.0 and Prandtl-Meyer expansion values for the shadowed parts of the booster, the theory agrees well with lift and drag coefficients up to about 20^o angle of attack. However, both coefficients were underpredicted as angle of attack was increased. Good agreement was obtained for L/D generally over the angle-of-attack range. Theory gave poor estimate of pitching-moment coefficient at angles of attack greater than 10^o as evidenced by the predicted trim angle of attack which was about 12^o higher than that measured.

Lateral directional.- The lateral-directional stability characteristics over the Mach number range for the booster are presented in figure 5. Positive effective dihedral $\left(-C_{l_\beta}\right)$ is indicated at the lower angles of attack at low subsonic speed and for all angles tested at the other Mach numbers. The booster was directionally stable over most of the angle-of-attack range tested at Mach numbers up to 0.70. At supersonic speeds, however, stability existed only at the lower angle-of-attack ranges; for instance, instability began to occur at 8^o angle of attack for M = 2.86 (fig. 5(g)). At M = 10.4, the booster was directionally unstable over the entire angle-of-attack range. Newtonian theory (fig. 5(h)) gave good estimates of the data trends at angles of attack up to about 30^o.

Longitudinal trim.- In figure 6, booster longitudinal trim characteristics are presented for Mach 0.28, 0.60, and 10.4. The results at the subsonic speeds were obtained

by interpolation procedures. A trimmed $(L/D)_{max}$ of 7.1 was obtained at $M = 0.28$ for an elevon setting of -13.7^{o} occurring at 7.5^{o} angle of attack. A Mach number increase to 0.60 reduced the trimmed $(L/D)_{max}$ to 6.5 at 6^{o} angle of attack. At Mach 10.4, a trimmed $(L/D)_{max}$ of 1.55 was obtained near 20^{o} angle of attack for a 0^{o} elevon setting. Deflecting the elevons to -20^{o} resulted in trim at a $C_{L,max}$ of 0.63 occurring at about 50^{o} angle of attack.

Ascent Configuration Characteristics

Longitudinal.- The longitudinal stability characteristics of the ascent configuration from 0.28 to 10.4 are presented in figure 7. During ascent flight, the center of gravity moves rearward considerably because of fuel consumption. The estimated center of gravity at lift-off ($x/l = 0.45$ and $z/l = 0.02$) was used as the moment reference center for the subsonic and supersonic tests. The moment reference center used for the hypersonic tests was the burnout center of gravity ($x/l = 0.741$ and $z/l = 0.066$). Minimum drag occurs near -3^{o} angle of attack over the Mach number range. Stability levels are unaffected as speed increased in the subsonic range; however, a destabilizing effect is indicated as Mach number increased to 2.86. With the rearward shift in center of gravity with M that would occur operationally, instantaneous static margins would have to be calculated to ascertain how much, if any, stability augmentation would be required. At Mach 10.4, this configuration is unstable based on the burnout center of gravity and augmentation could be required at burnout.

Lateral directional.- The lateral-directional stability parameters are presented in figure 8 at Mach 0.28 to 2.86. Positive dihedral effect was obtained for angles of attack up to at least 15^{o}. Decreases in directional stability occurred as Mach number increased from 1.50 to 2.86.

Interference Drag

In the design of a two-stage shuttle system, the aerodynamic drag of the ascent configuration and that part of the total drag ascribed to mutual interference effect from lift-off to staging is significant in obtaining booster performance. The energy required to overcome ascent drag losses represents a velocity increment of about 232 m/sec (760 ft/sec) of a total increment of about 9.5 km/sec (31 000 ft/sec) for a system with a 15.2-MN (3.4-million-pound) lift-off weight. (See ref. 1.) Nearly 90 percent of these drag losses occur at Mach numbers below 3.0. The limited data available to date indicate that the drag of the mated orbiter and booster usually exceeds the sum of the two vehicles from isolated tests. For the present configuration, however, the drag of the ascent configuration exceeded the drag of the isolated components by as much as 50 percent at Mach numbers below 2.0 and up to a 15-percent reduction was measured

at Mach 10 (figs. 9 and 10). Drag coefficients for the orbiter were obtained from references 9 to 13.

By using a calculated ascent trajectory, integrated values of interference drag represented by the K parameter of figure 10 resulted in losses of 14 and 28.7 m/sec (46 and 94 ft/sec) greater than those for interference-free drag (K = 1) for angles of attack of -5° and 4°, respectively. By using the sensitivity values of reference 1, the corresponding increases in gross lift-off weight are 0.11 to 0.22 MN (24 300 to 49 600 pounds) for a constant payload weight. Based on a constant gross lift-off weight, this translates into a payload reduction of 2.4 and 4.8 percent.

During ascent flight, the actual angle of attack will vary with fuel expenditure and speed. For the rocket thrust passing through the center of gravity, the angle of attack will be positive. For this condition, ascent drag and losses will be greatest for the angles of attack shown in figure 11; however, the values of K for these same angles are smallest (fig. 10).

CONCLUSIONS

A wind-tunnel investigation was conducted at Langley Research Center on a two-stage shuttle concept similar to that studied recently for the NASA. Longitudinal and lateral-directional stability characteristics were obtained for the booster and the ascent configurations over a Mach number range of 0.28 to 10.4. The following results were obtained from this investigation:

1. The booster was longitudinally and laterally stable over the planned operational flight regimes and was directionally stable at Mach numbers up to 0.70. At supersonic speeds, directional stability was limited to lower ranges of angle of attack while at hypersonic speeds, instability occurred over the entire angle-of-attack range.

2. At trim conditions, a maximum lift-drag ratio of about 7 was obtained at low subsonic speeds at a Reynolds number of 11.4×10^6 based on model length. A trim maximum lift coefficient of 0.63 was measured at about 50° angle of attack at Mach 10.4.

3. The ascent configuration was longitudinally unstable at nominal staging conditions (Mach 10.4).

4. Interference drag losses for the ascent configuration are highly sensitive to angles of attack and represent as much as a 4.8-percent reduction in payload for a 15.2-MN (3.4-million-pound) lift-off weight.

Langley Research Center,
National Aeronautics and Space Administration,
Hampton, Va., April 16, 1971.

REFERENCES

1. Anon.: Integral Launch and Reentry Vehicle Systems. Vols. I to IV. MDC E0049 (Contract NAS 9-9204), McDonnell Douglas Astronautics Co., Eastern Div., Nov. 1969. (Available as NASA CR-66863-1, CR-66863-2, CR-66864, CR-66865, and CR-66866.)

2. Schaefer, William T.: Characteristics of Major Active Wind Tunnels at the Langley Research Center. NASA TM X-1130, 1965.

3. Anon.: Manual for Users of the Unitary Plan Wind Tunnel Facilities of the National Advisory Committee for Aeronautics. NACA, 1956.

4. Dunavant, James C.; and Stone, Howard W.: Effect of Roughness on Heat Transfer to Hemisphere Cylinders at Mach Numbers 10.4 and 11.4. NASA TN D-3871, 1967.

5. Braslow, Albert L.; and Knox, Eugene C.: Simplified Method for Determination of Critical Height of Distributed Roughness Particles for Boundary-Layer Transition at Mach Numbers From 0 to 5. NACA TN 4363, 1958.

6. Gillis, Clarence L.; Polhamus, Edward C.; and Gray, Joseph L., Jr.: Charts for Determining Jet-Boundary Corrections for Complete Models in 7- by 10-Foot Closed Rectangular Wind Tunnels. NACA WR L-123, 1945. (Formerly NACA ARR L5G31.)

7. Herriot, John G.: Blockage Corrections for Three-Dimensional-Flow Closed-Throat Wind Tunnels With Consideration of the Effect of Compressibility. NACA Rep. 995, 1950. (Supersedes NACA RM A7B28.)

8. Gentry, Arvel E.: Hypersonic Arbitrary-Body Aerodynamic Computer Program. Vol. I – User's Manual. Rep. DAC 56080 (Air Force Contract No. F33615 67 C 1008), Douglas Aircraft Co., Mar. 1967. (Available from DDC as AD 817 158.)

9. Spencer, Bernard, Jr.; and Fox, Charles H., Jr.: Subsonic Longitudinal Control Characteristics of Several Elevon Configurations for a Manned Lifting Entry Vehicle. NASA TM X-1227, 1966.

10. Harris, Charles D.: Transonic Aerodynamic Characteristics of a Manned Lifting Entry Vehicle With and Without Tip Fins. NASA TM X-1248, 1966.

11. Campbell, James F.; and Watson, Carolyn B.: Stability and Control, Hinge-Moment, and Pressure-Coefficient Data for the HL-10 Manned Lifting Entry Vehicle at Mach Numbers From 1.41 to 2.16. NASA TM X-1300, 1966.

12. Ladson, Charles L.: Aerodynamic Characteristics of a Manned Lifting Entry Vehicle With Modified Tip Fins at Mach 6.8. NASA TM X-1158, 1965.

13. Ladson, Charles L.: Aerodynamic Characteristics of the HL-10 Manned Lifting Entry Vehicle at a Mach Number of 10.5. NASA TM X-1504, 1968.

TABLE I.- GEOMETRIC CHARACTERISTICS OF BOOSTER MODELS

Large Model

Length	40.64 cm (16 in.)
Total planform area	0.0595 m^2 (0.641 ft^2)
Wing span	31.55 cm (12.42 in.)
Wing total area	0.0466 m^2 (0.502 ft^2)
Aspect ratio	2.13
Leading-edge sweep angle	55^o
Root chord at model center line	26.01 cm (10.24 in.)
Tip chord	3.54 cm (1.392 in.)
Dihedral angle	15^o
Taper ratio	0.136
Vertical tail area	0.0059 m^2 (0.0636 ft^2)
Vertical tail sweep angle	50^o
Elevon total area	0.0087 m^2 (0.0934 ft^2)

Small Model

Length	25.4 cm (10 in.)
Total planform area	0.0233 m^2 (0.2504 ft^2)
Wing span	19.71 cm (7.76 in.)
Wing total area	0.0182 m^2 (0.196 ft^2)
Root chord at model center line	16.28 cm (6.41 in.)
Tip chord	2.21 cm (0.87 in.)
Vertical tail area	0.0023 m^2 (0.0248 ft^2)
Elevon total area	0.0034 m^2 (0.0365 ft^2)

TABLE II.- TEST CONDITIONS

Facility	Configuration	M	p_o		T_o		R_l	α range	β
			kN/m2	psia	°K	°R		deg	deg
Low-turbulence pressure tunnel	Large booster	0.28	482	70	Ambient		[a]11.4×10^6	-8 to 26	0, 5
	Ascent	↓	↓	↓	↓		↓	-8 to 16	↓
High-speed 7- by 10-foot tunnel	Large booster	0.40 .60 .70	101	14.7	Ambient		3.3×10^6 4.5 4.7	-8 to 40	0
		0.40 .60 .70					3.3×10^6 4.5 4.7	3 to 40	±3
	Ascent	0.40 .60 .70 .85					3.3×10^6 4.5 4.7 5.2	-8 to 16	0
		0.40 .60 .70 .85					3.3×10^6 4.5 4.7 5.2	3 to 16	±3
Unitary Plan wind tunnel	Large booster	1.50 2.16 2.86	79.9 102 147	11.6 14.9 21.4	339	610	4.0×10^6	-10 to 25	0, 3
	Ascent	1.50 2.16 2.86	79.9 102 147	11.6 14.9 21.4				-8 to 16	
Continuous-flow hypersonic tunnel	Large booster	10.4	5170	750	994	1790	1.33×10^6	-2 to 29	0, 5
	Small booster		7230	1050	994	1790	1.15×10^6	30 to 59	0, 5
	Ascent		5170	750	1006	1810	1.33×10^6	-4 to 10	0

[a]Additional tests at R_l of 3.1×10^6 to 19.8×10^6 for $\delta_e = 0^o$ indicated negligible effects on slopes of C_L and $C_{m,s}$ up to 12^o angle of attack with $(L/D)_{max}$ values ranging from 7.35 to 7.55.

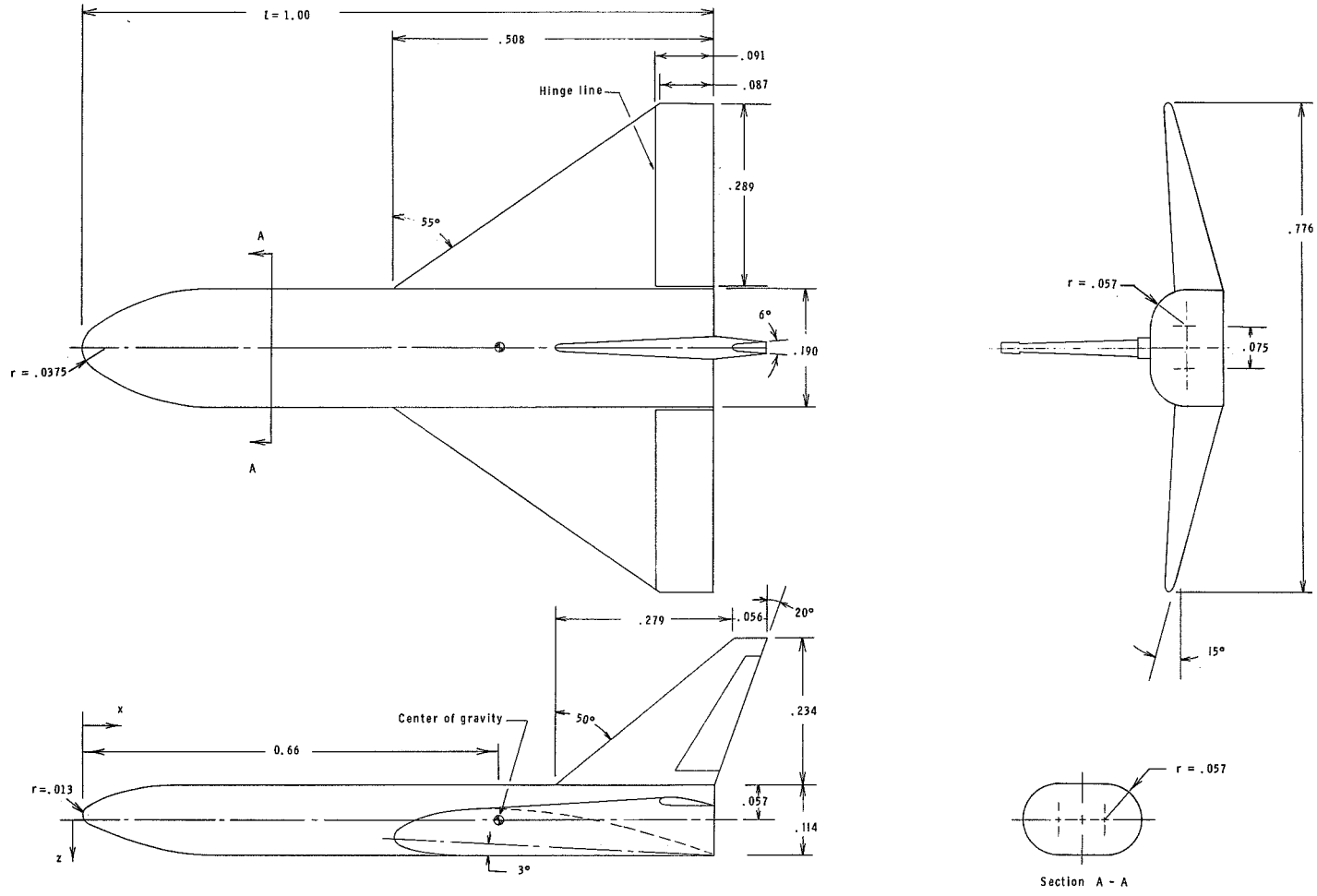

Figure 1.- Clipped-delta-wing booster. Linear dimensions are nondimensionalized by booster length ℓ.

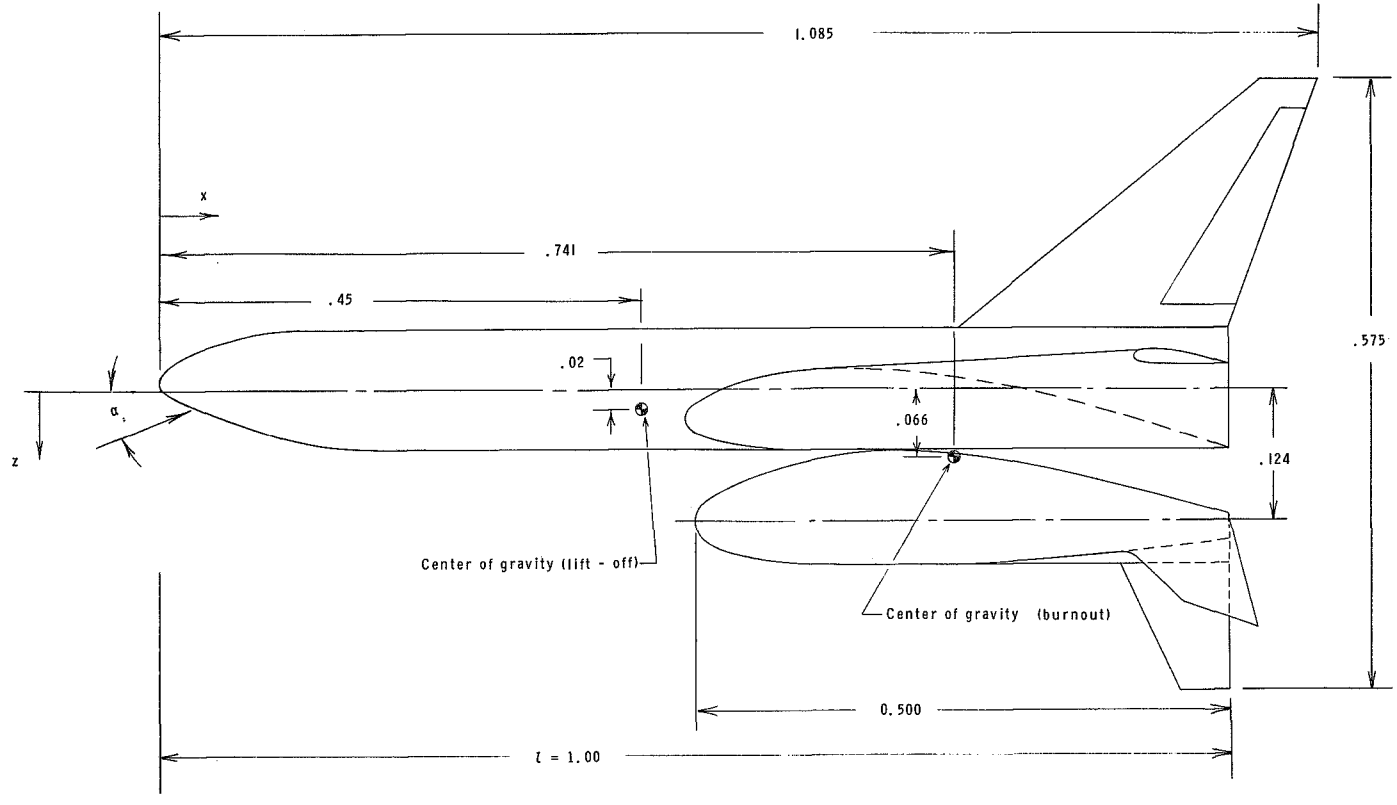

(a) Ascent configuration.

Figure 2.- Ascent-configuration details. Linear dimensions are nondimensionalized by booster length ℓ.

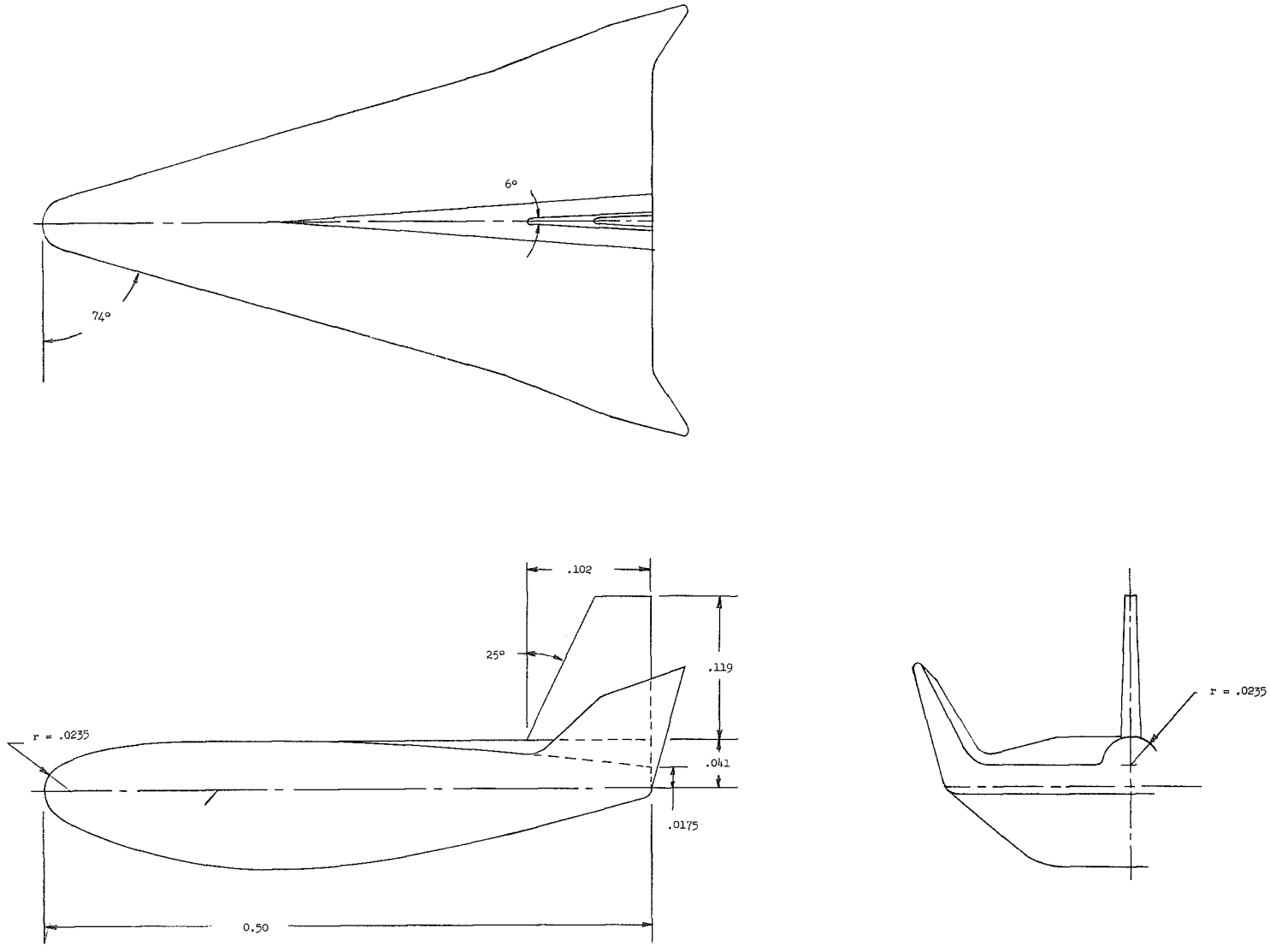

(b) Orbiter (HL-10).

Figure 2.- Concluded.

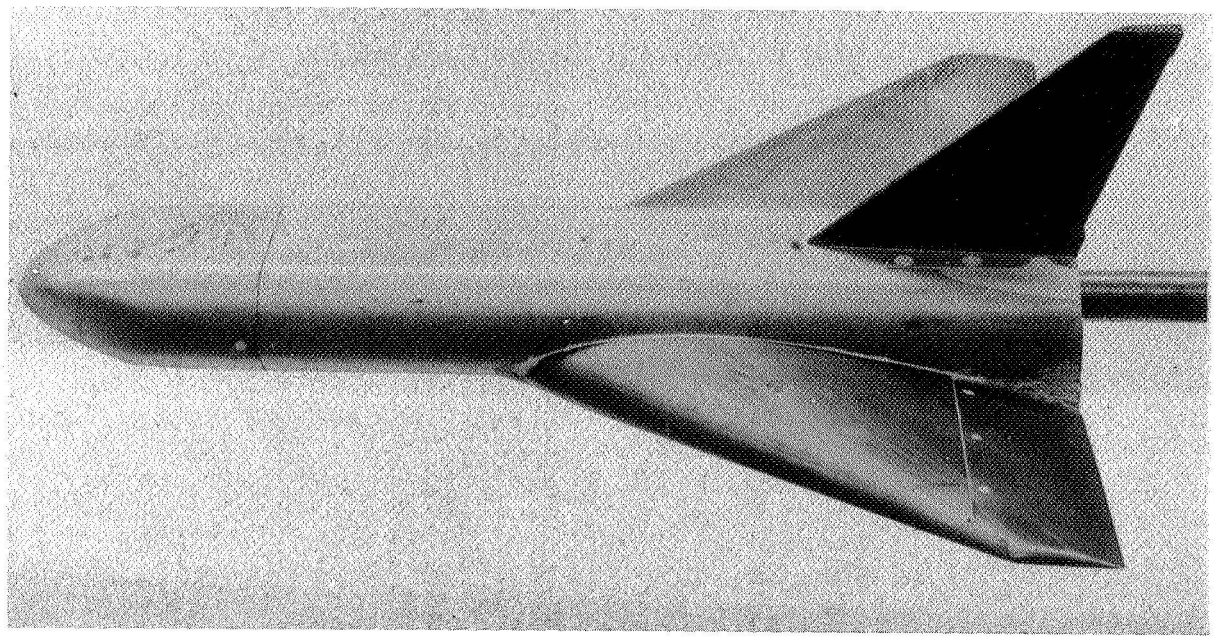

(a) Large booster model.

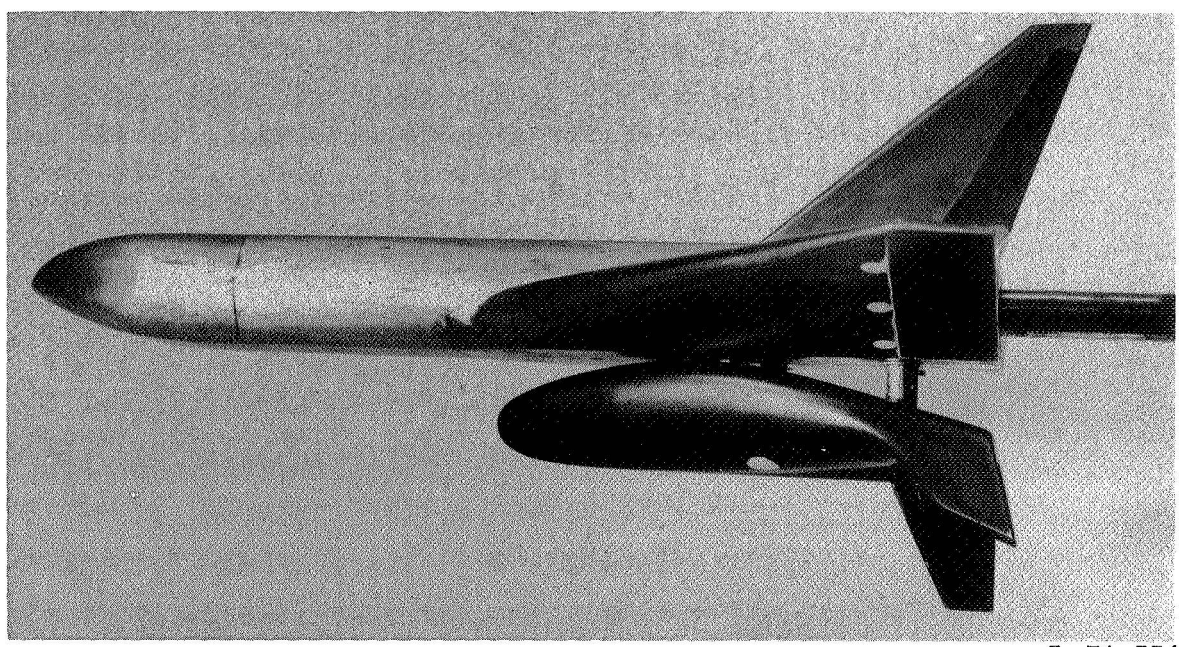

(b) Ascent configuration.

L-71-554

Figure 3.- Photographs of test configurations.

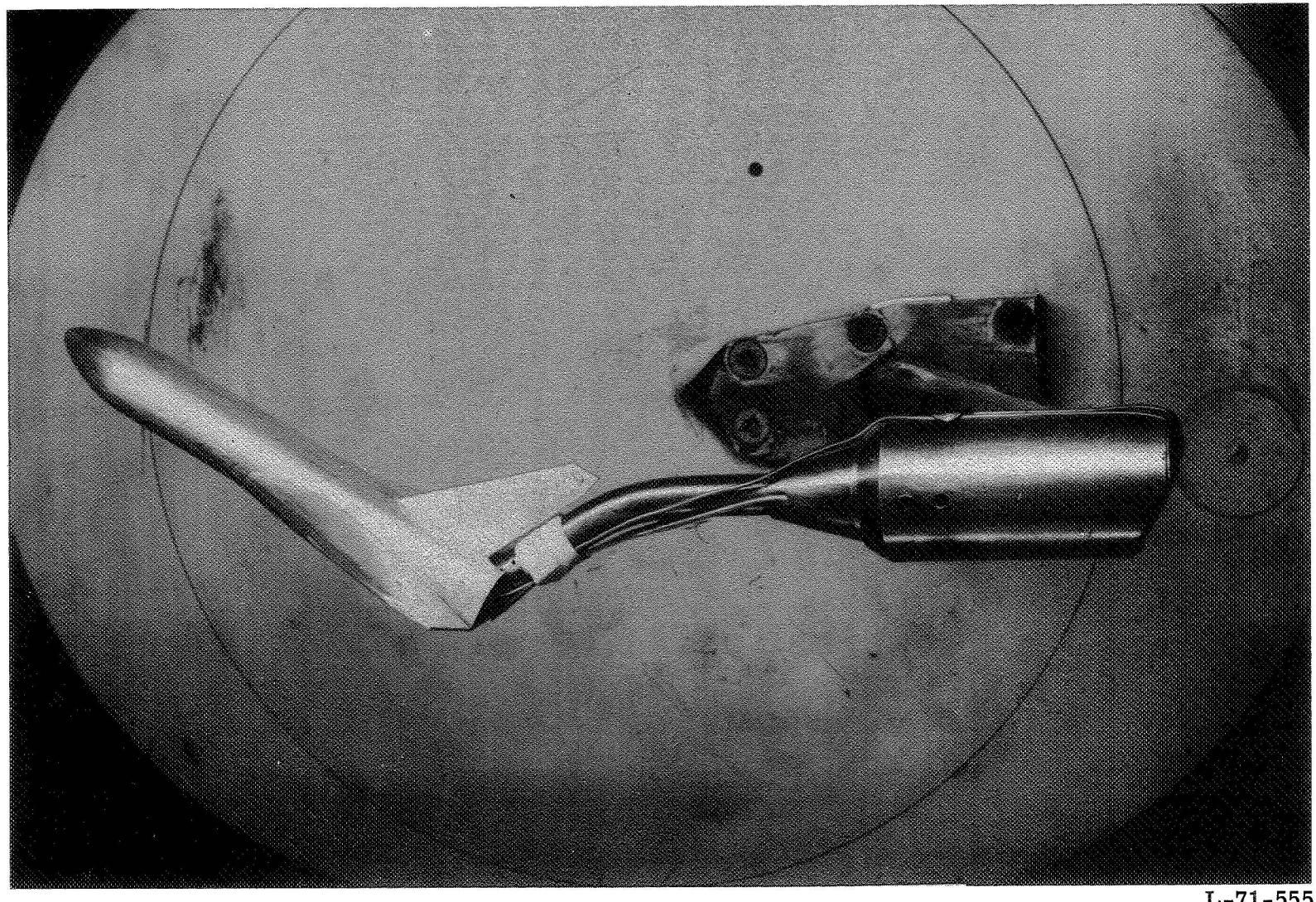

L-71-555

(c) Small booster model with bent sting.

Figure 3.- Concluded.

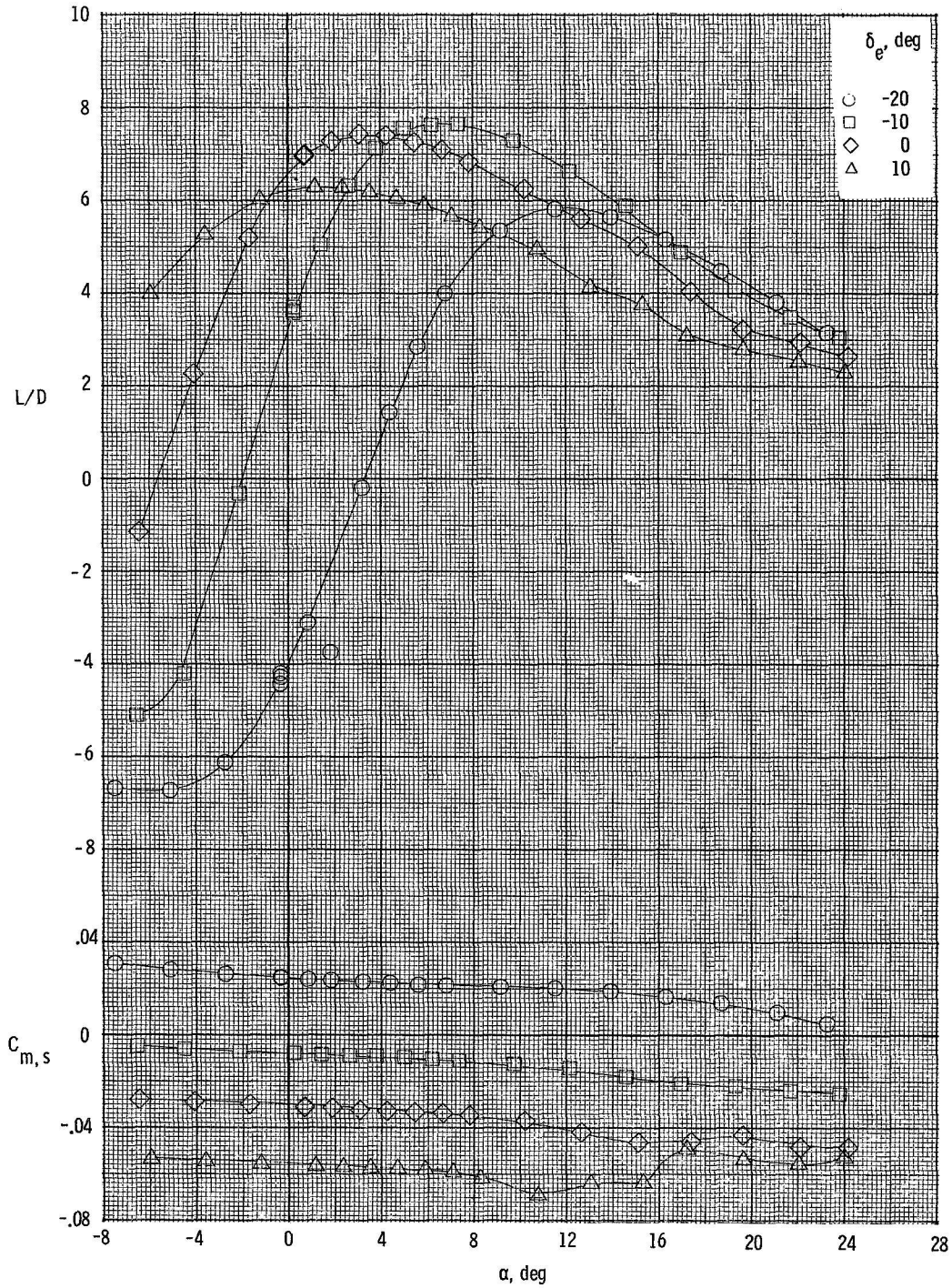

(a) M = 0.28; $R_\ell = 11.4 \times 10^6$.

Figure 4.- Longitudinal stability characteristics of booster for various elevon deflections. M = 0.28 to 10.4.

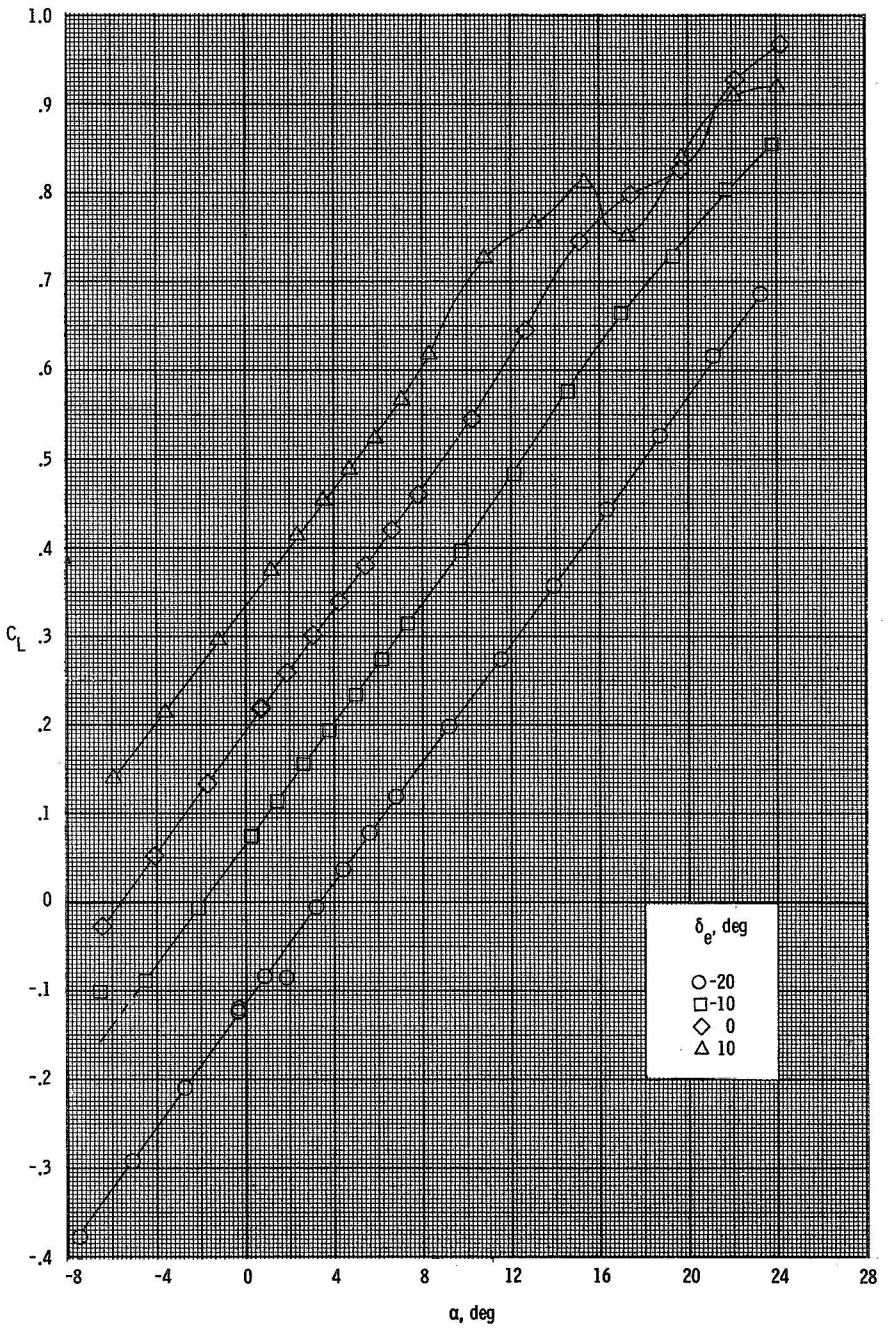

(a) Continued.

Figure 4.- Continued.

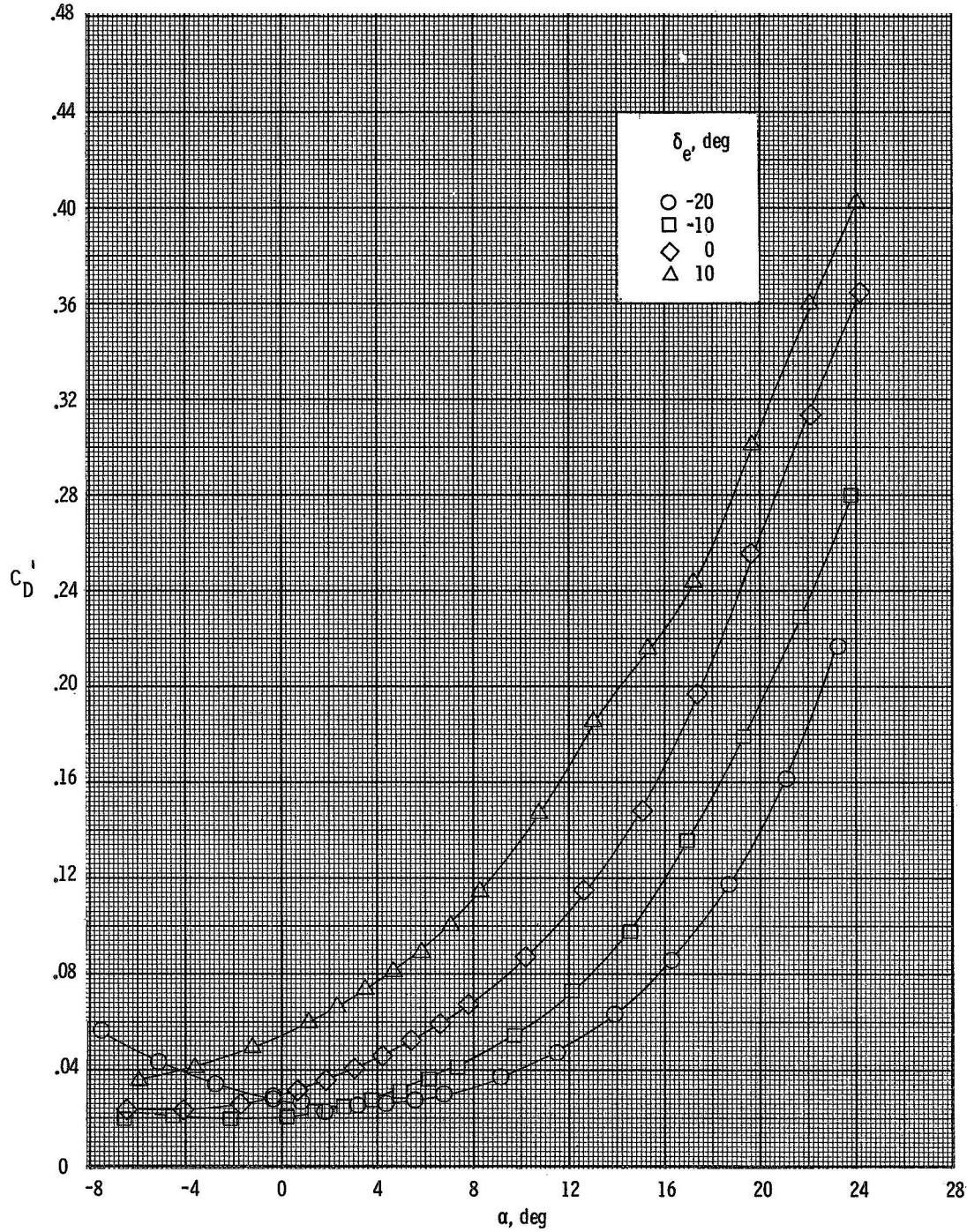

(a) Concluded.

Figure 4.- Continued.

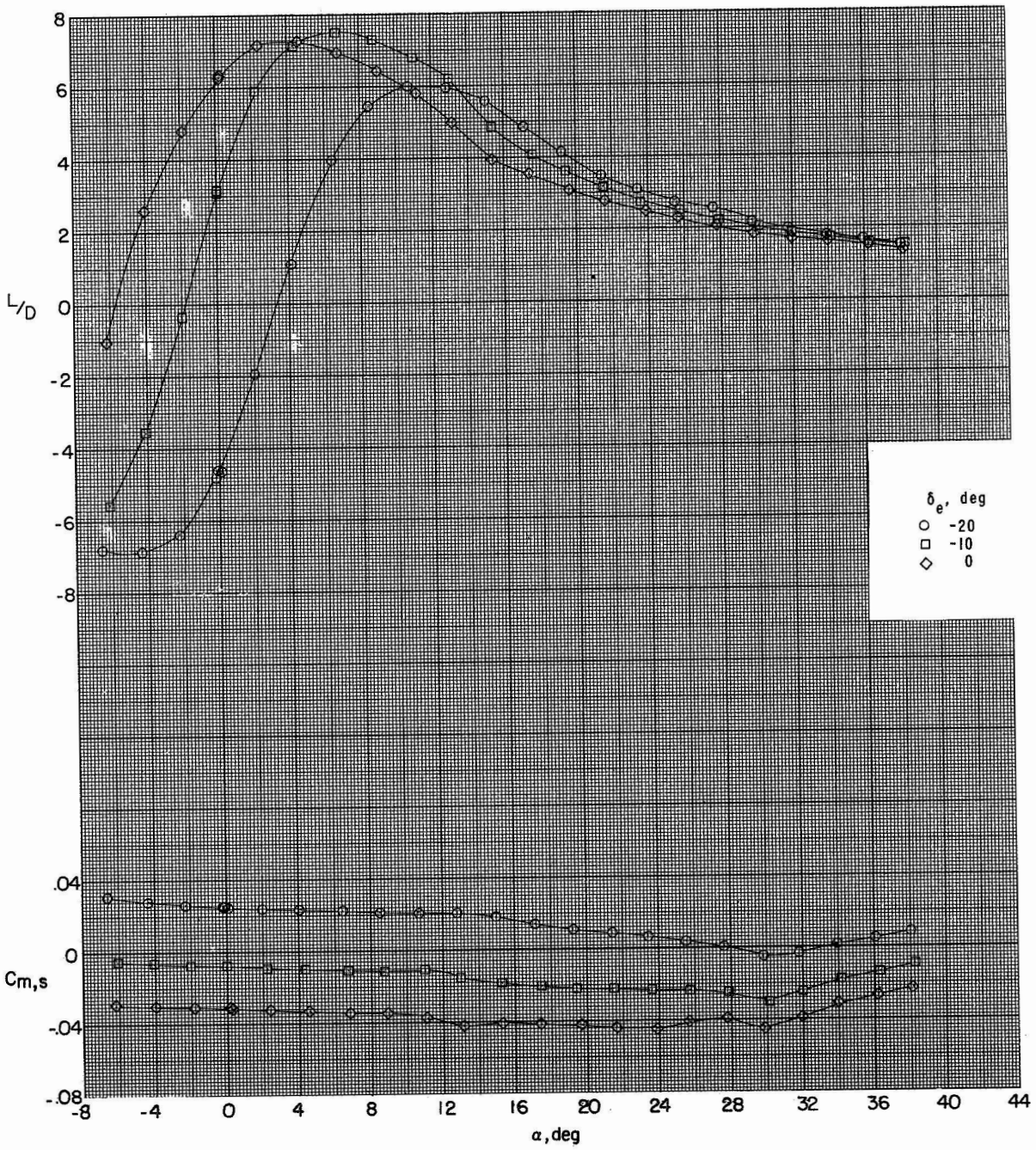

(b) M = 0.40; $R_l = 3.3 \times 10^6$.

Figure 4.- Continued.

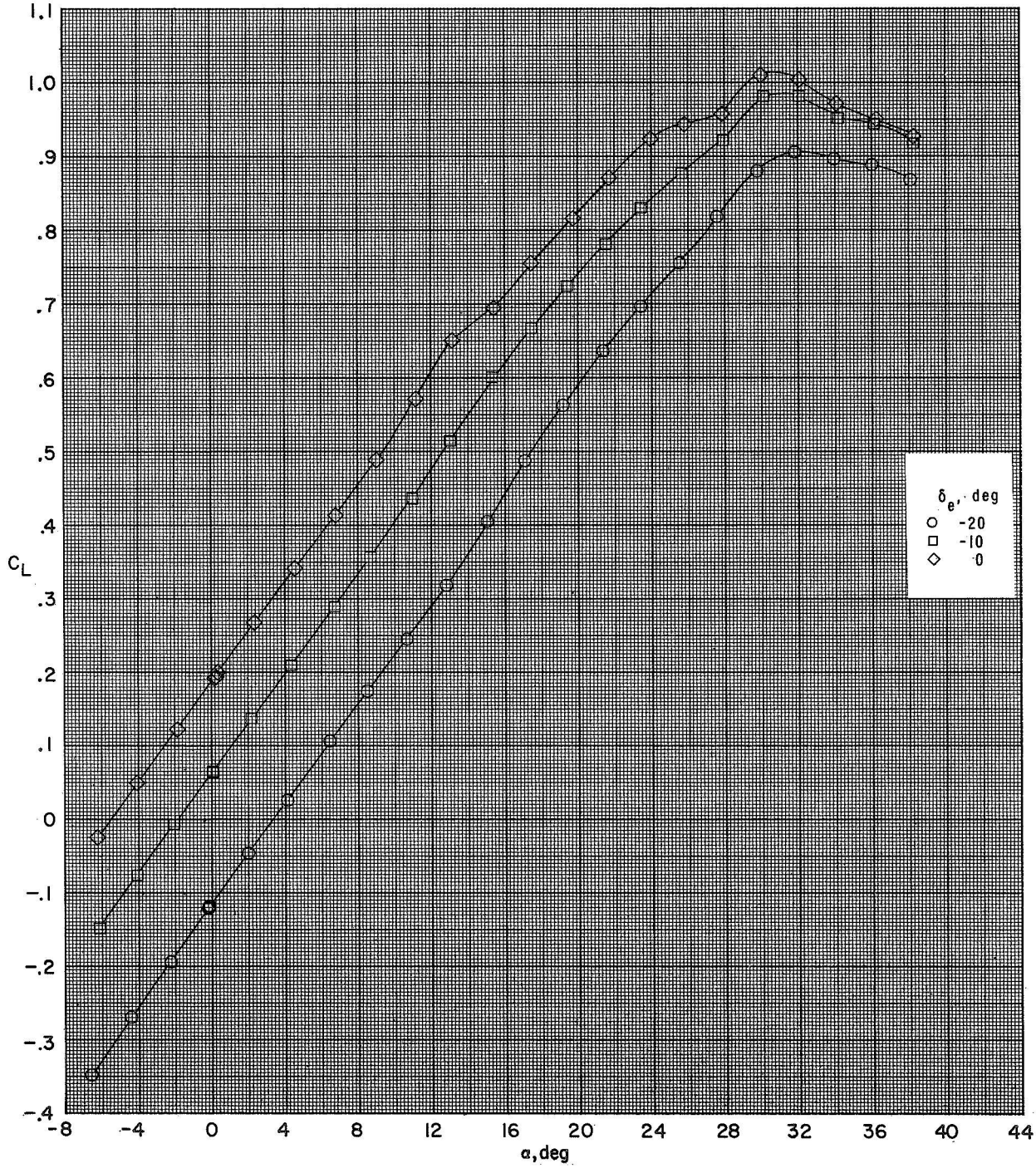

(b) Continued.

Figure 4.- Continued.

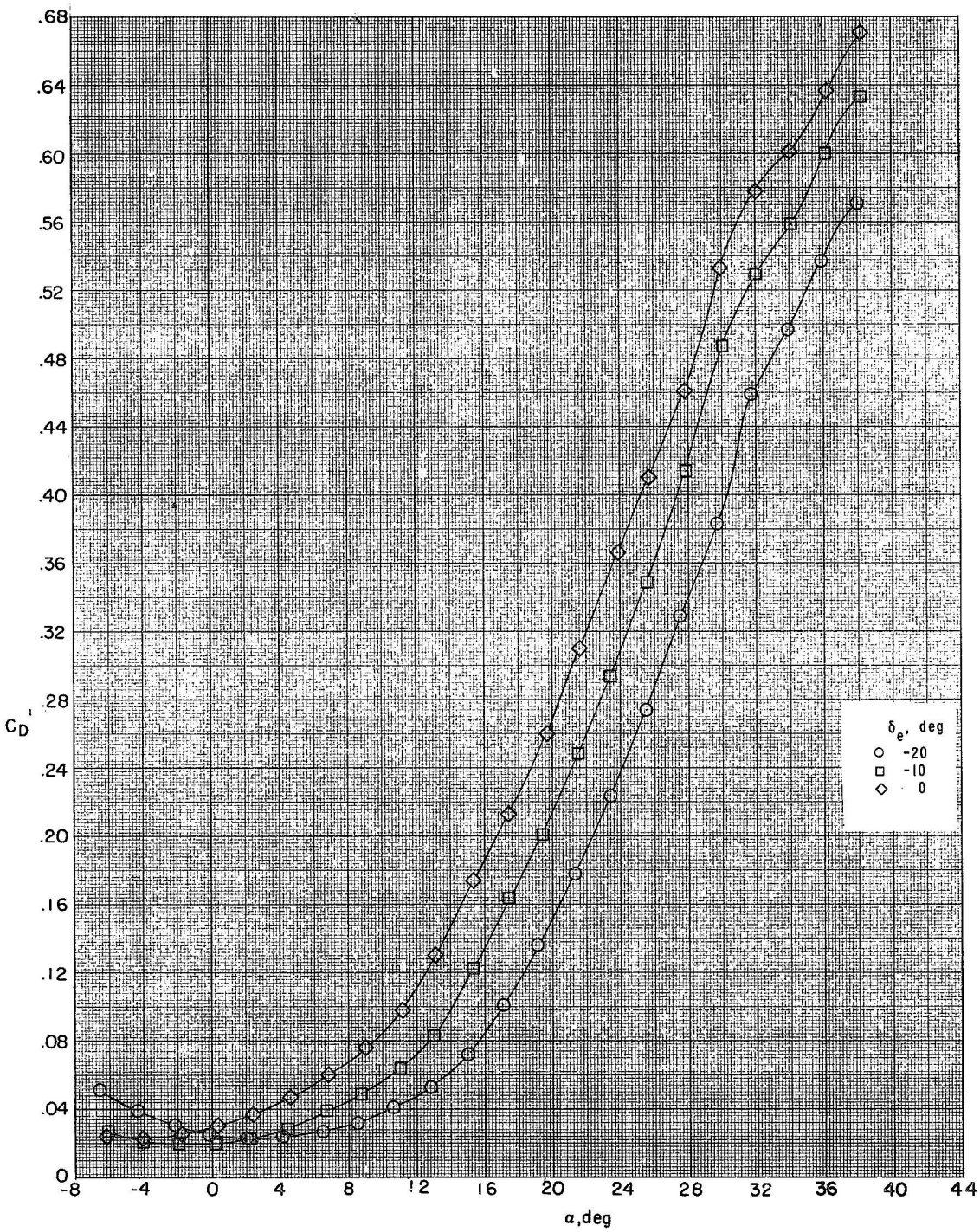

(b) Concluded.

Figure 4.- Continued.

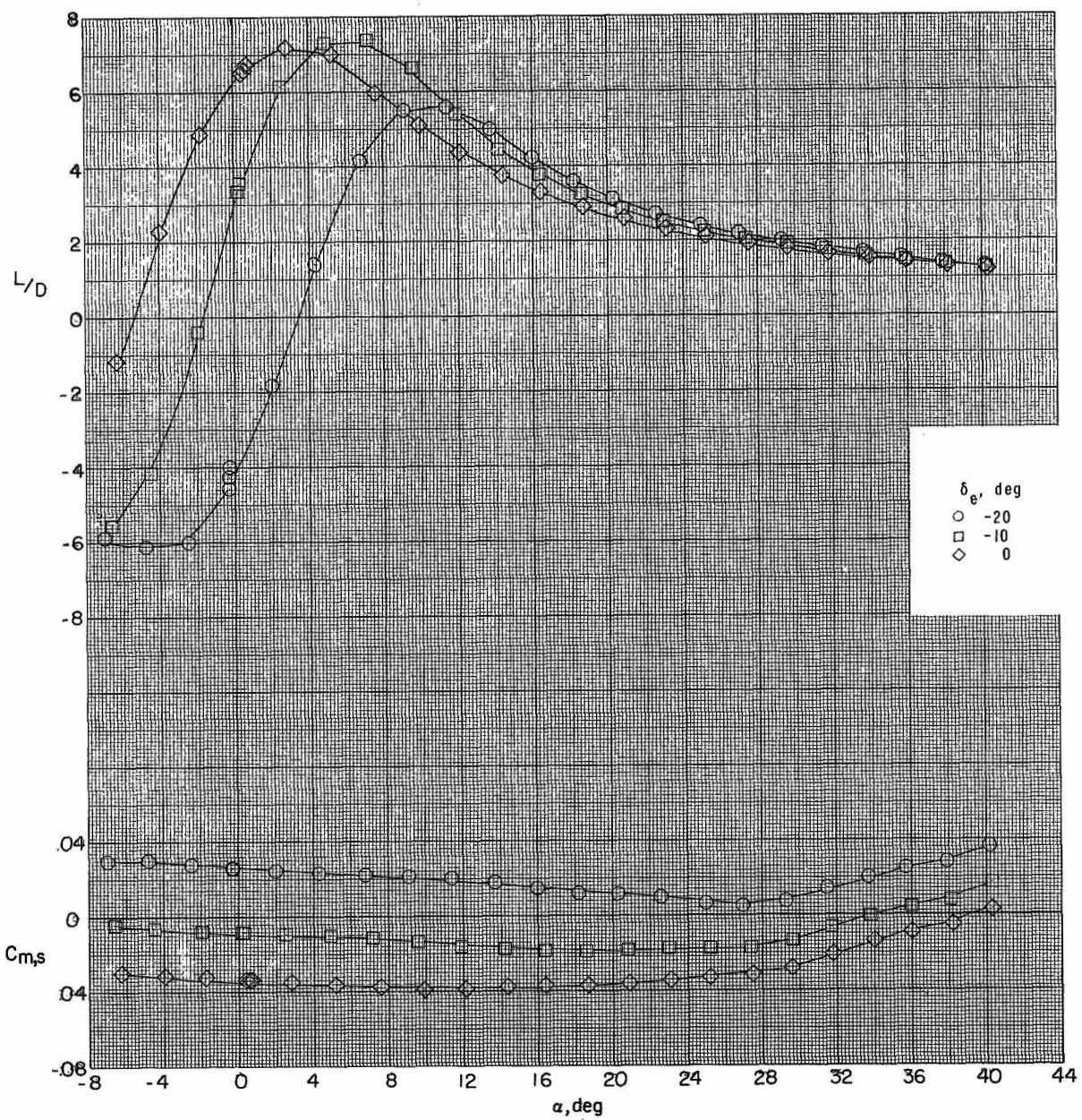

(c) $M = 0.60$; $R_l = 4.5 \times 10^6$.

Figure 4.- Continued.

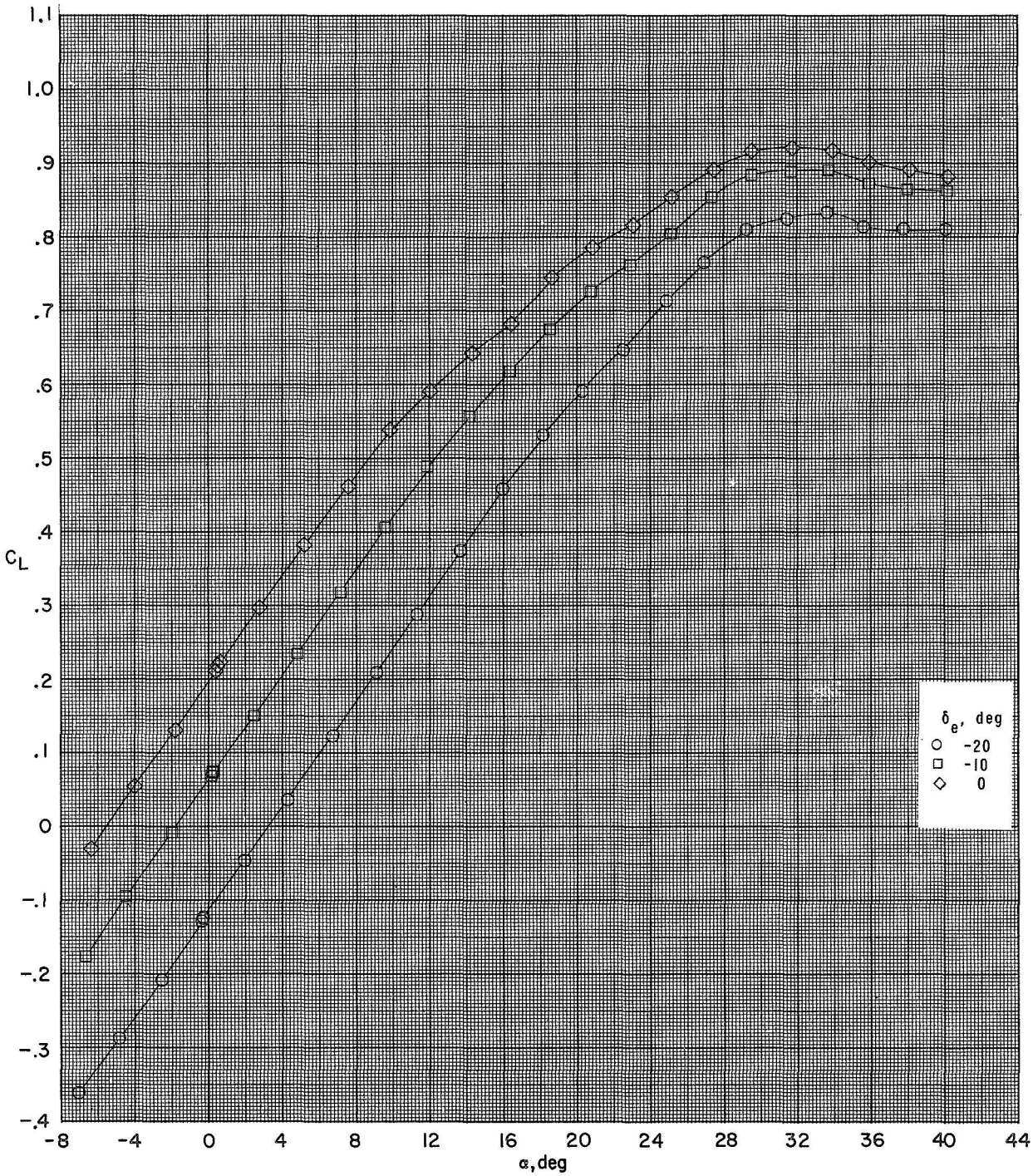

(c) Continued.

Figure 4.- Continued.

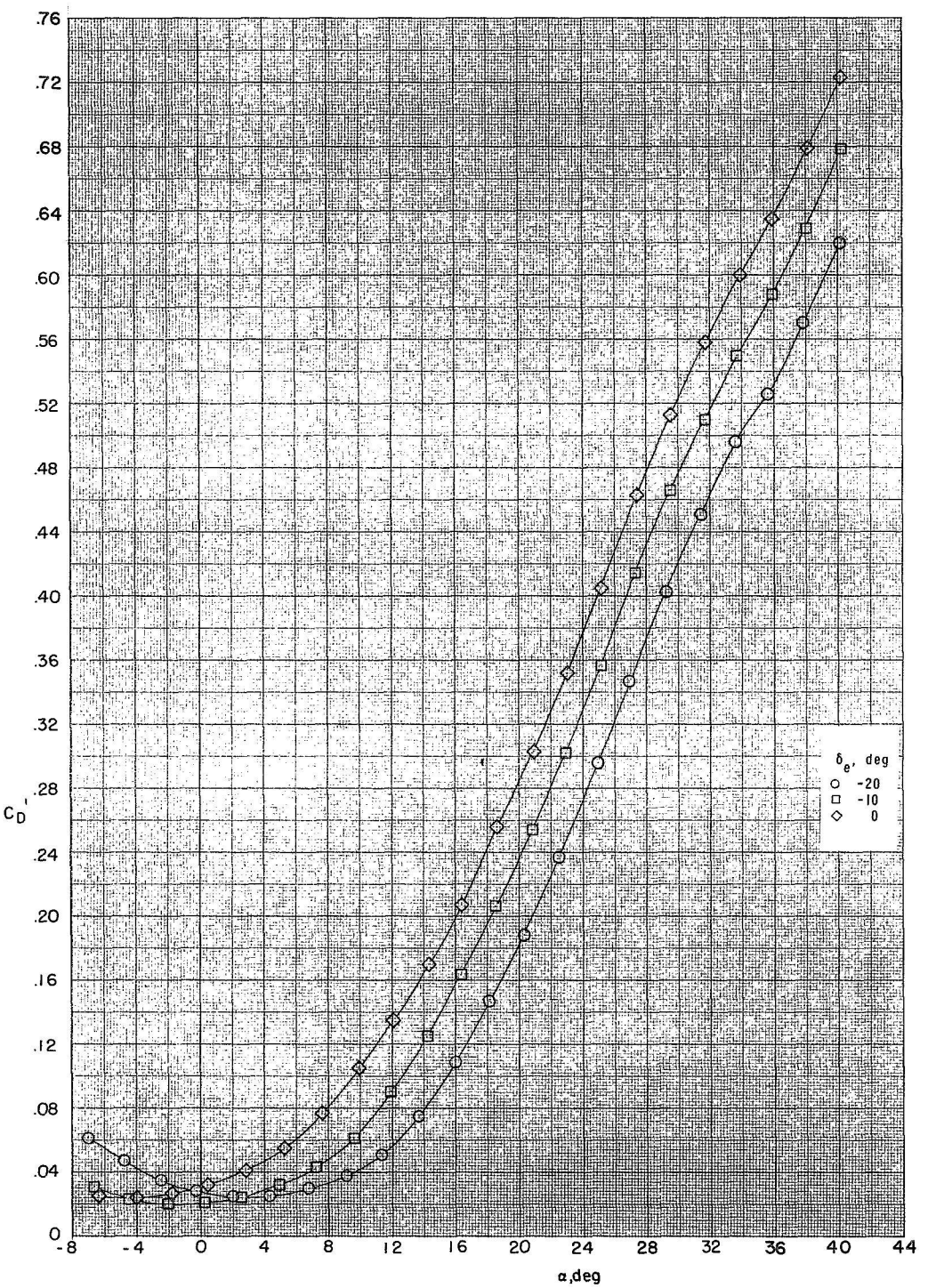

(c) Concluded.

Figure 4.- Continued.

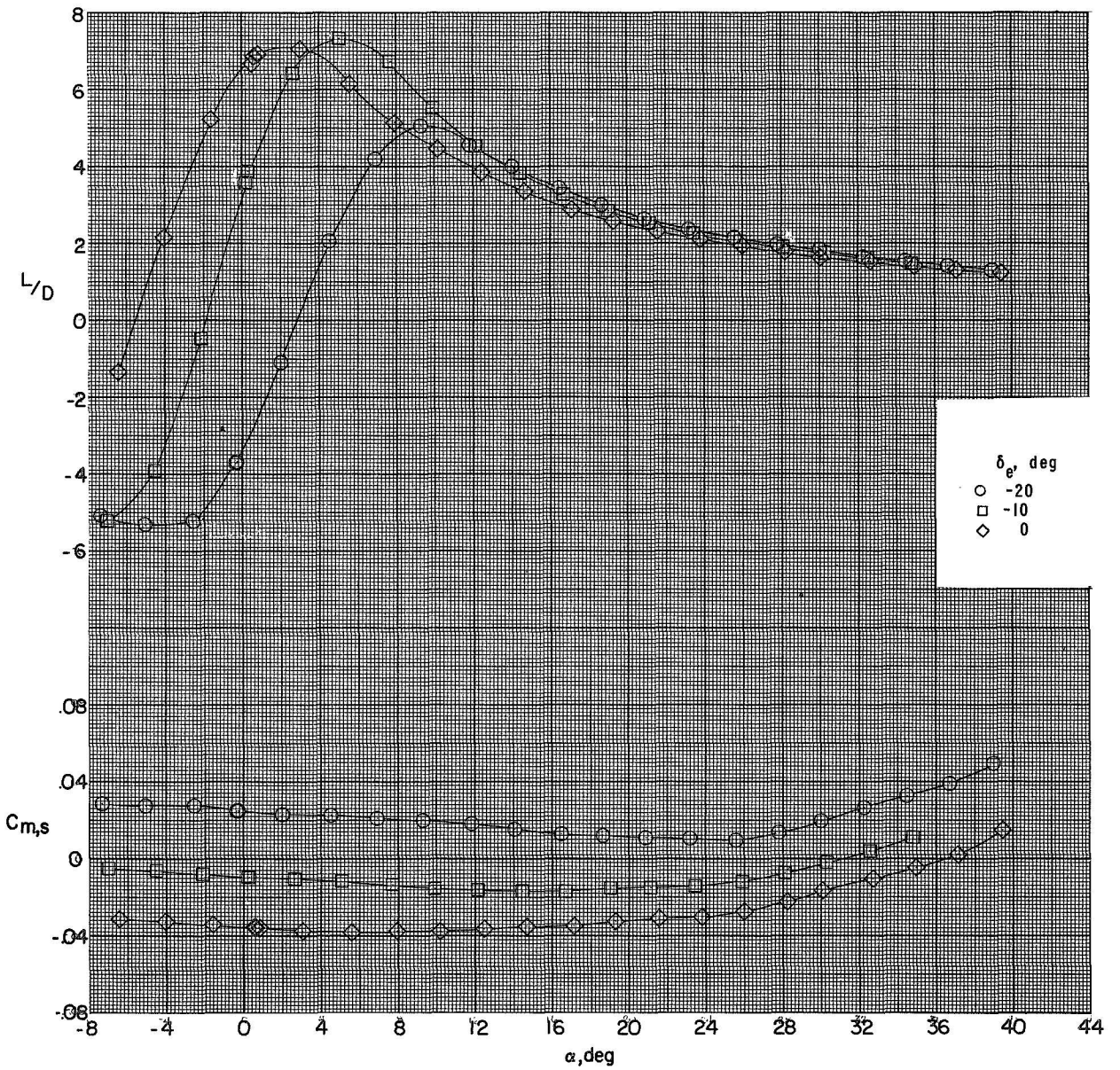

(d) $M = 0.70$; $R_l = 4.7 \times 10^6$.

Figure 4.- Continued.

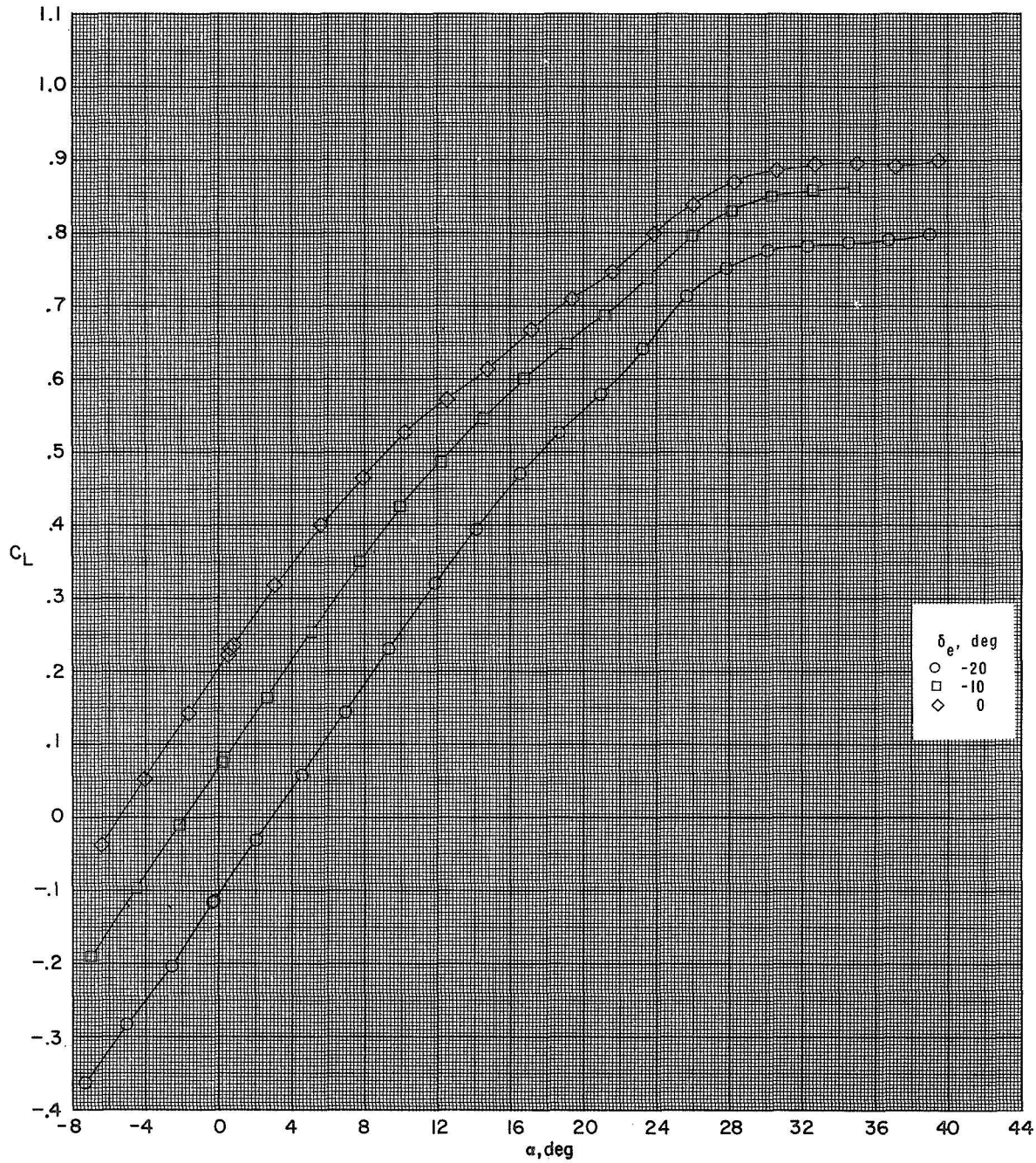

(d) Continued.

Figure 4.- Continued.

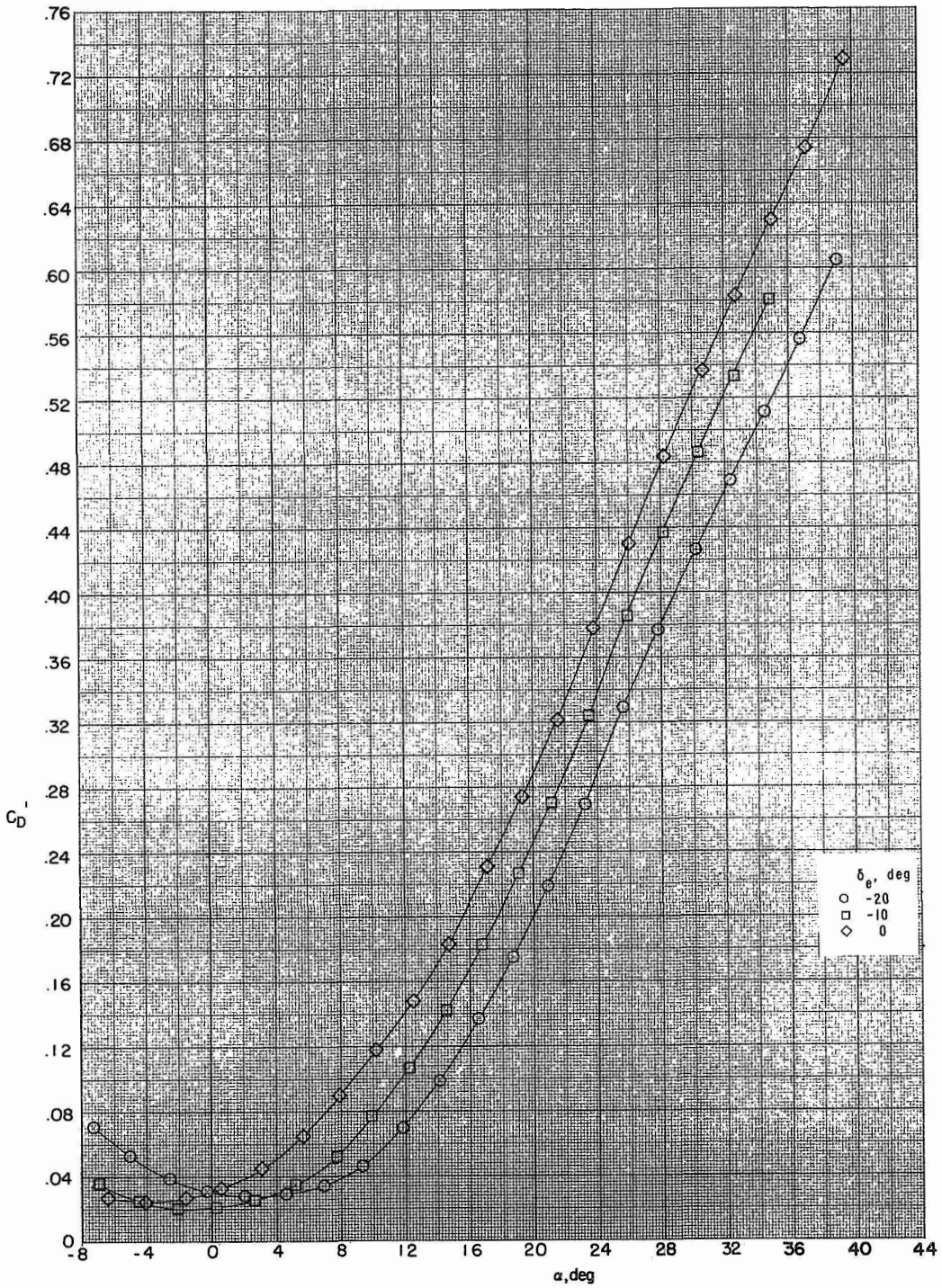

(d) Concluded.

Figure 4.- Continued.

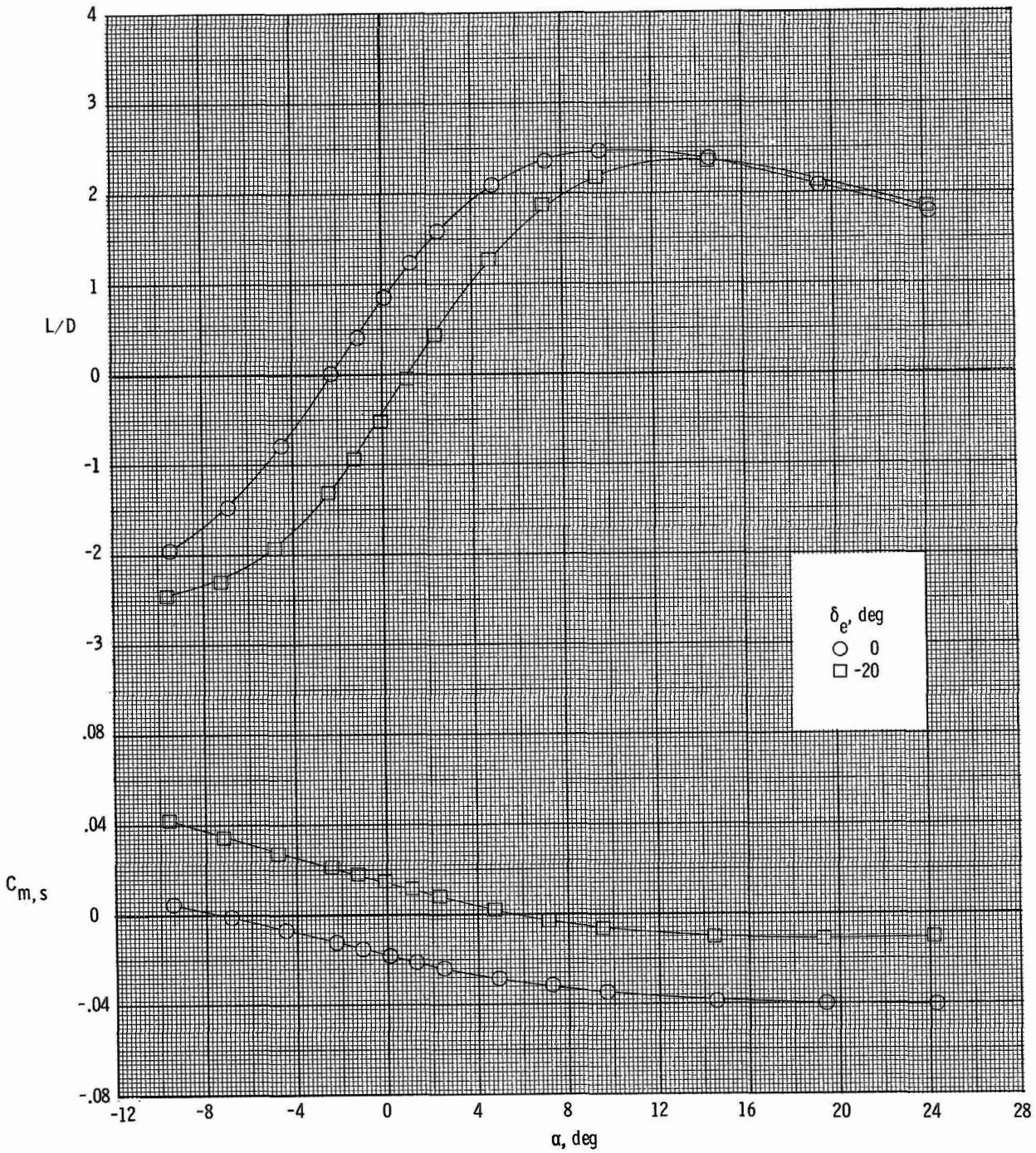

(e) M = 1.50; $R_\ell = 4.0 \times 10^6$.

Figure 4.- Continued.

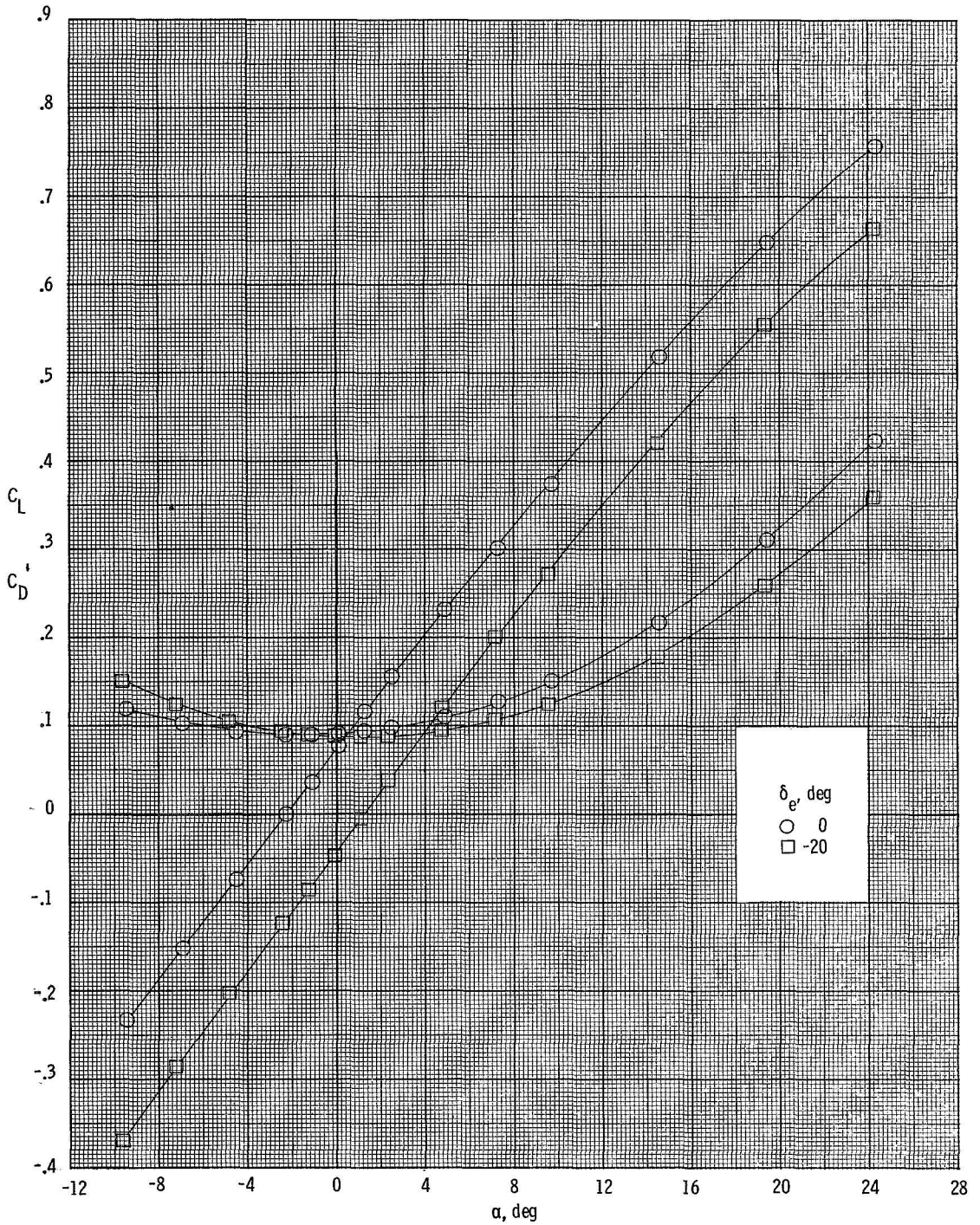

(e) Concluded.

Figure 4.- Continued.

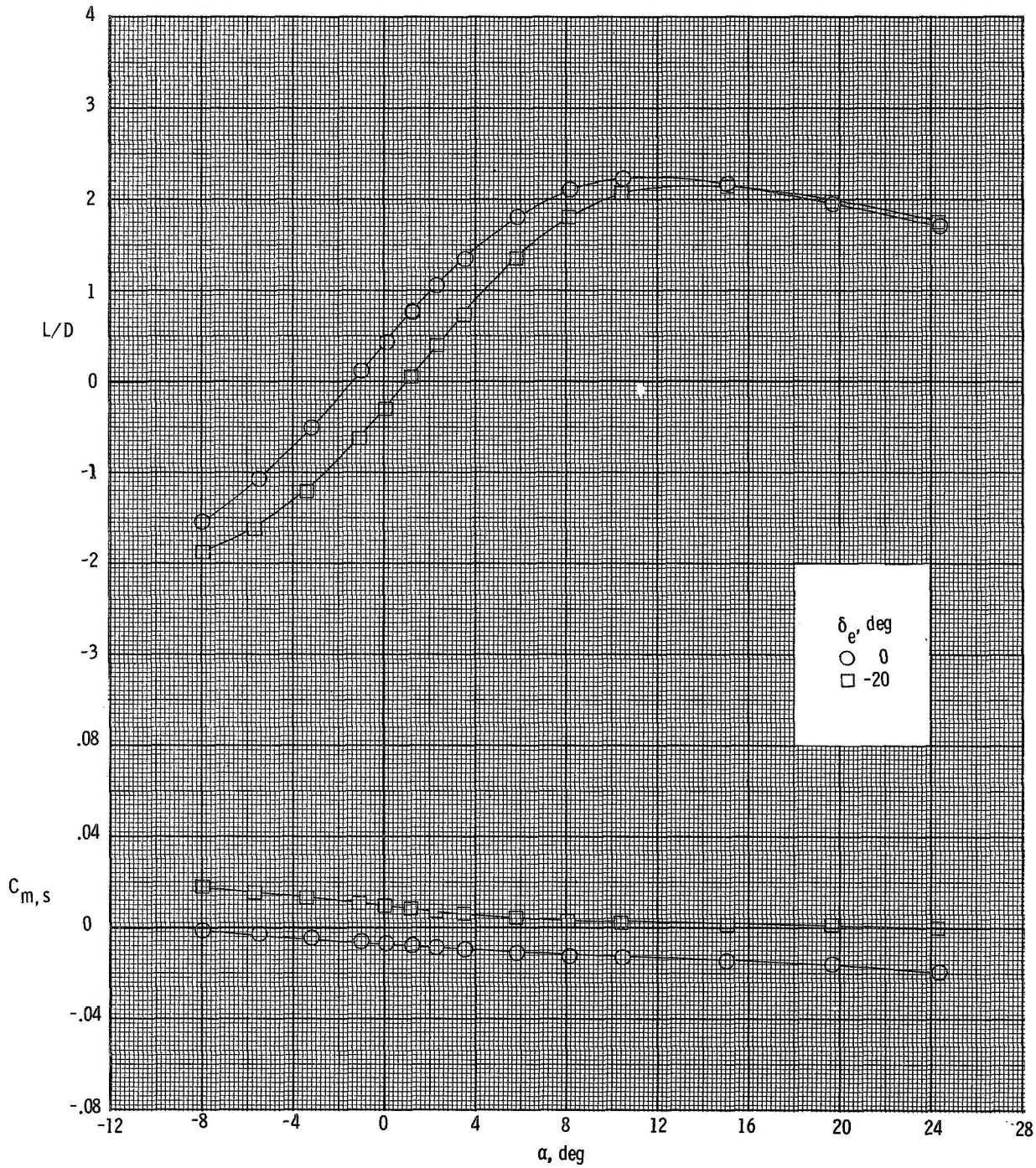

(f) M = 2.16; $R_l = 4.0 \times 10^6$.

Figure 4.- Continued.

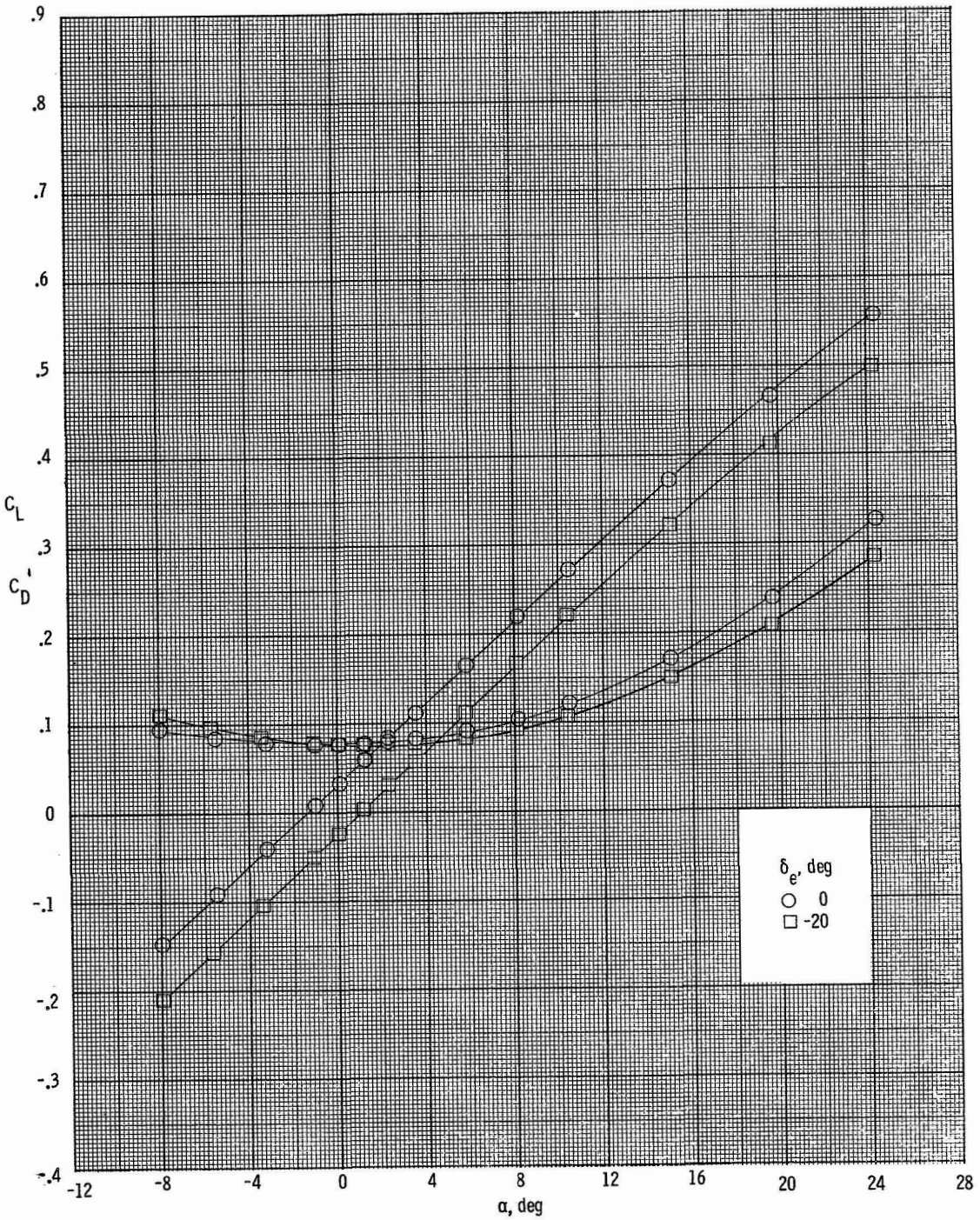

(f) Concluded.

Figure 4.- Continued.

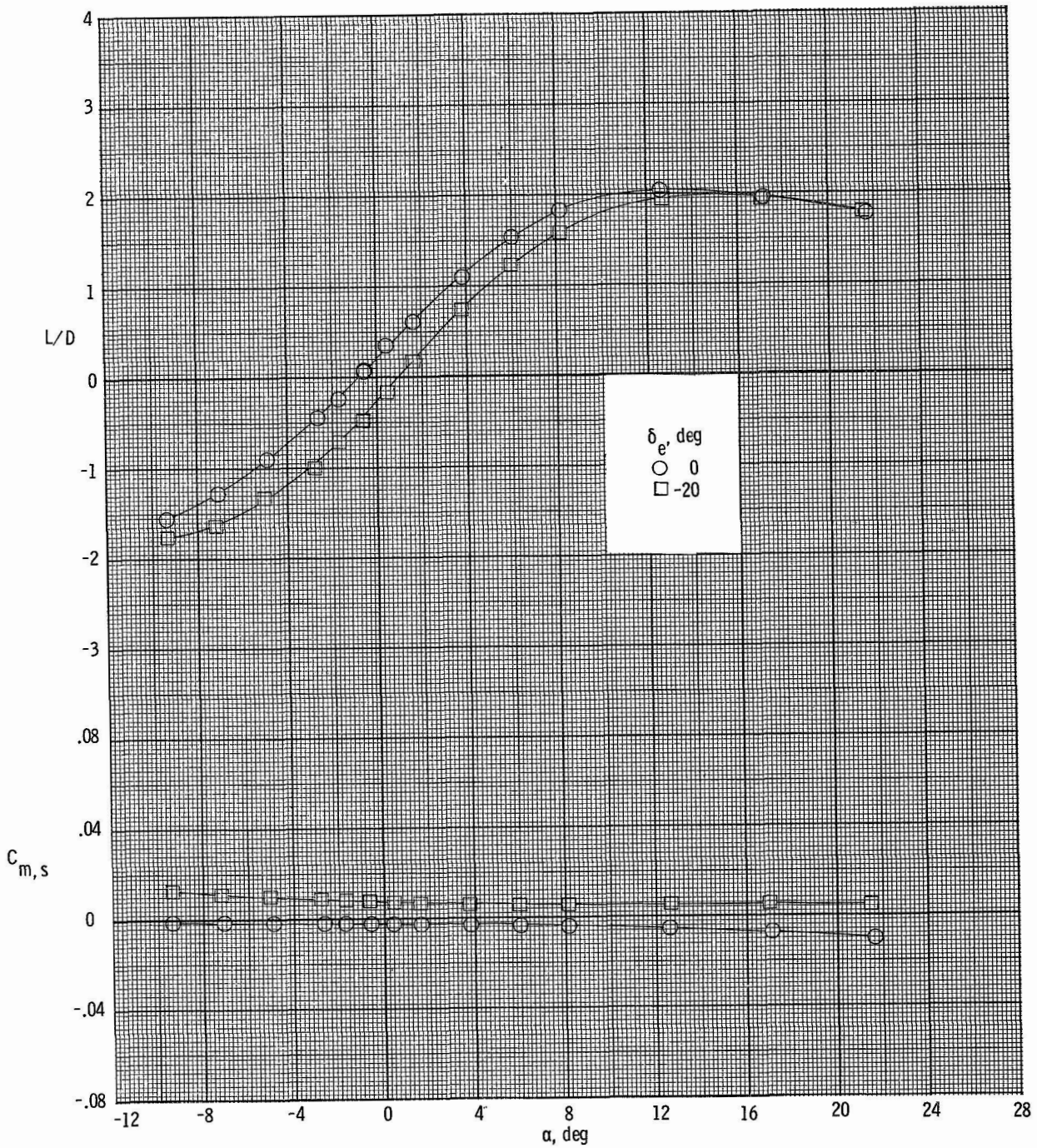

(g) M = 2.86; $R_l = 4.0 \times 10^6$.

Figure 4.- Continued.

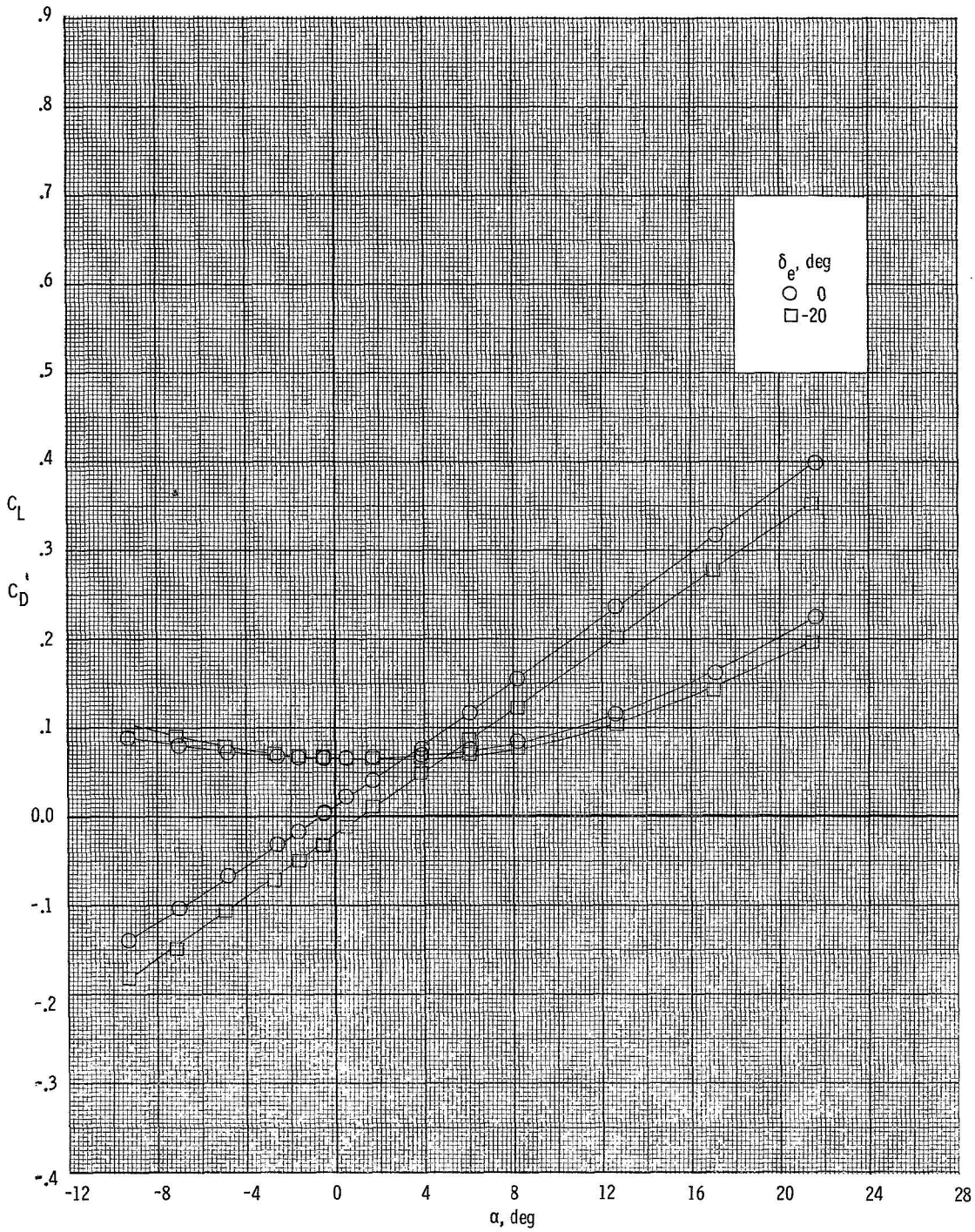

(g) Concluded.

Figure 4.- Continued.

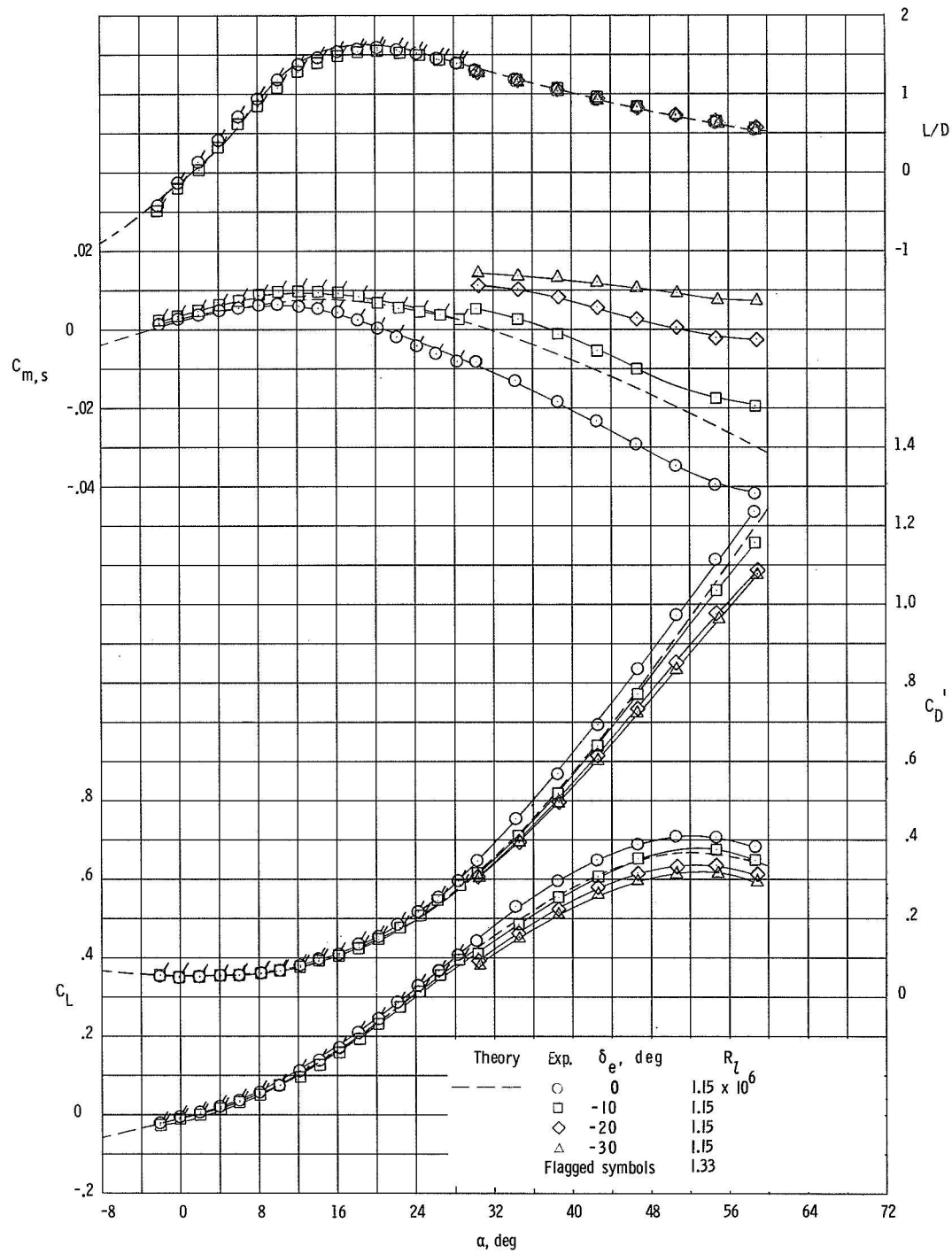

(h) M = 10.4.

Figure 4.- Concluded.

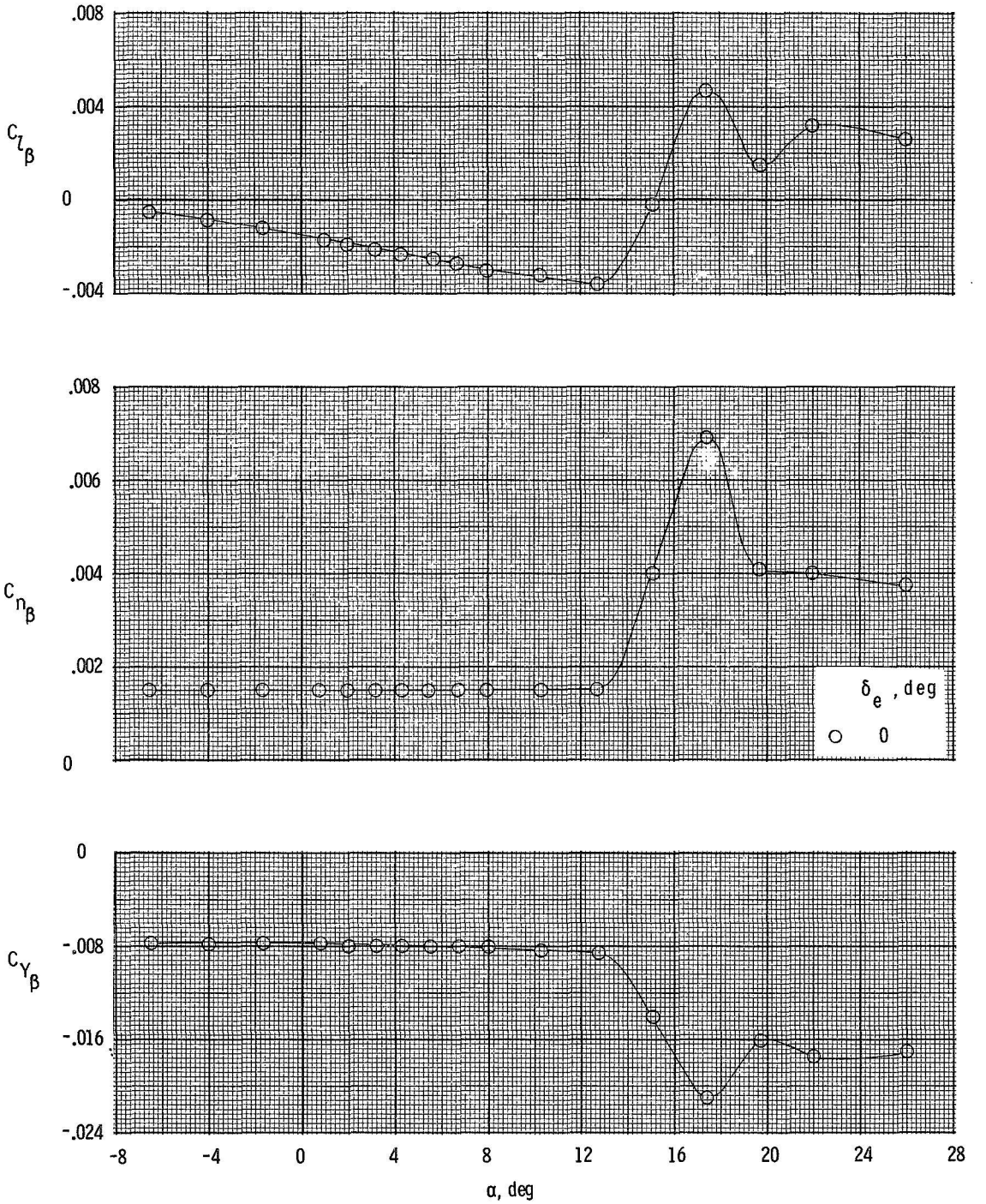

(a) M = 0.28; $R_l = 11.4 \times 10^6$.

Figure 5.- Lateral-directional stability characteristics of booster for various elevon deflections. M = 0.28 to 10.4.

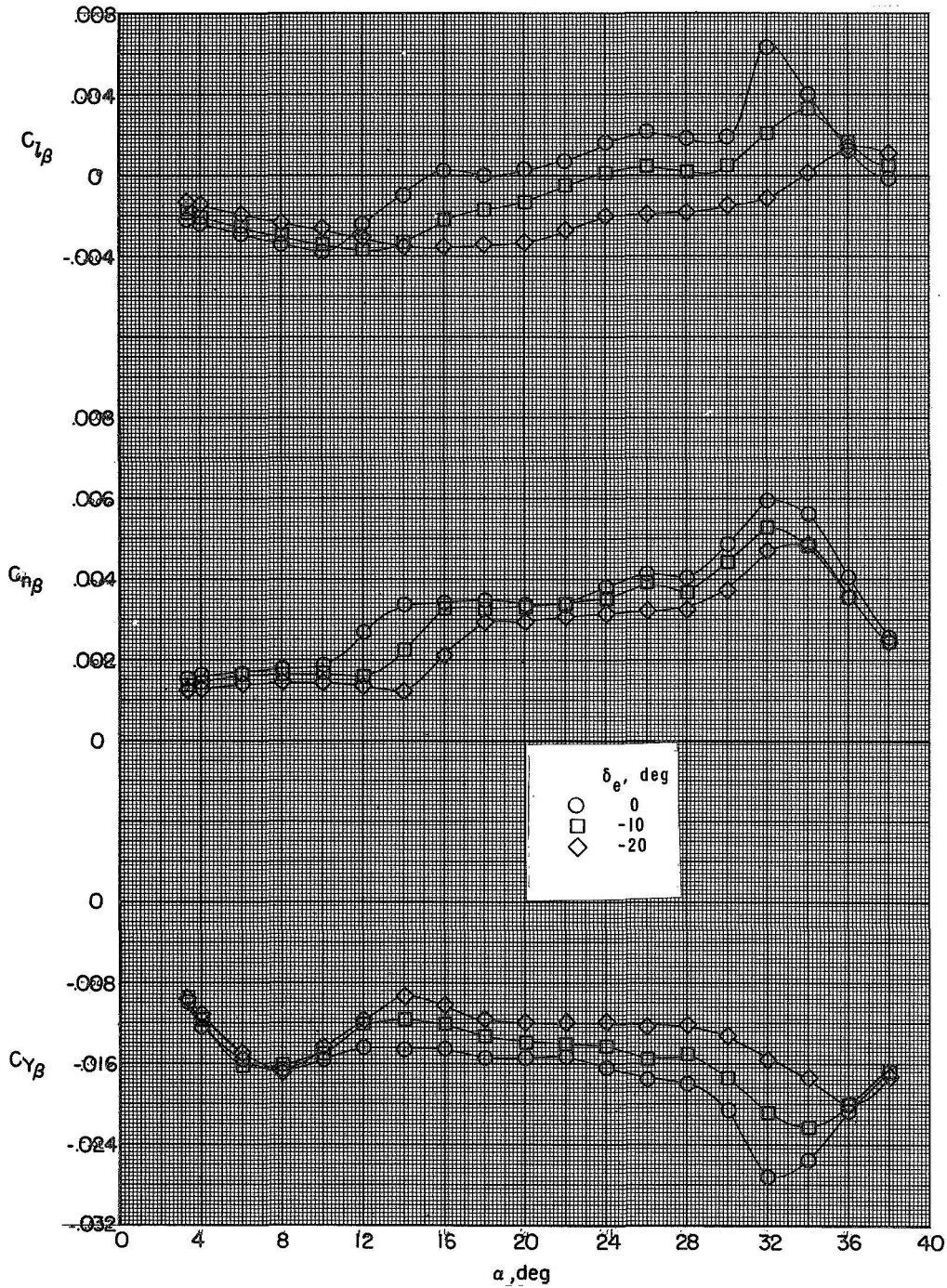

(b) M = 0.40; $R_l = 3.3 \times 10^6$.

Figure 5.- Continued.

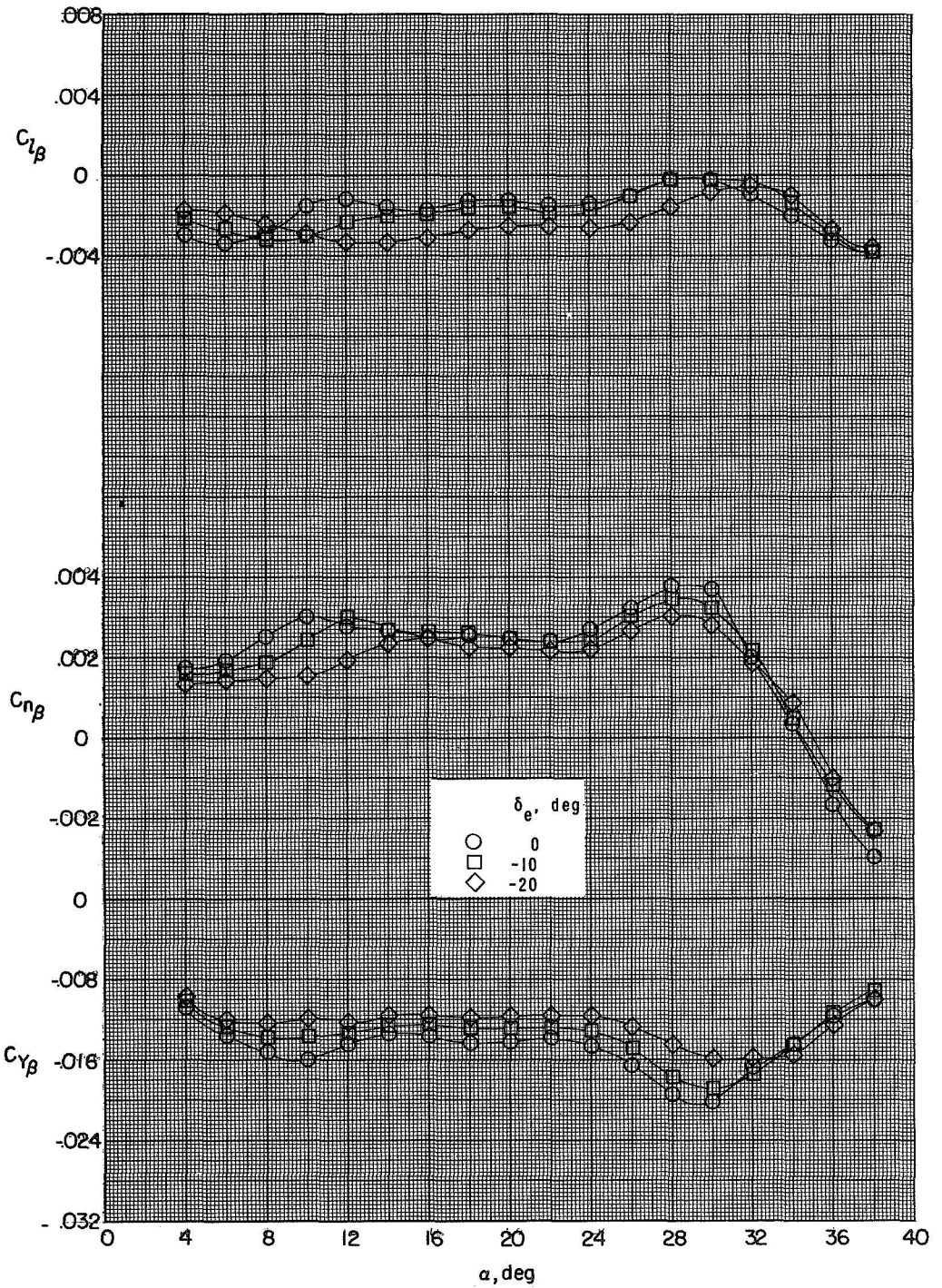

(c) M = 0.60; $R_l = 4.5 \times 10^6$.

Figure 5.- Continued.

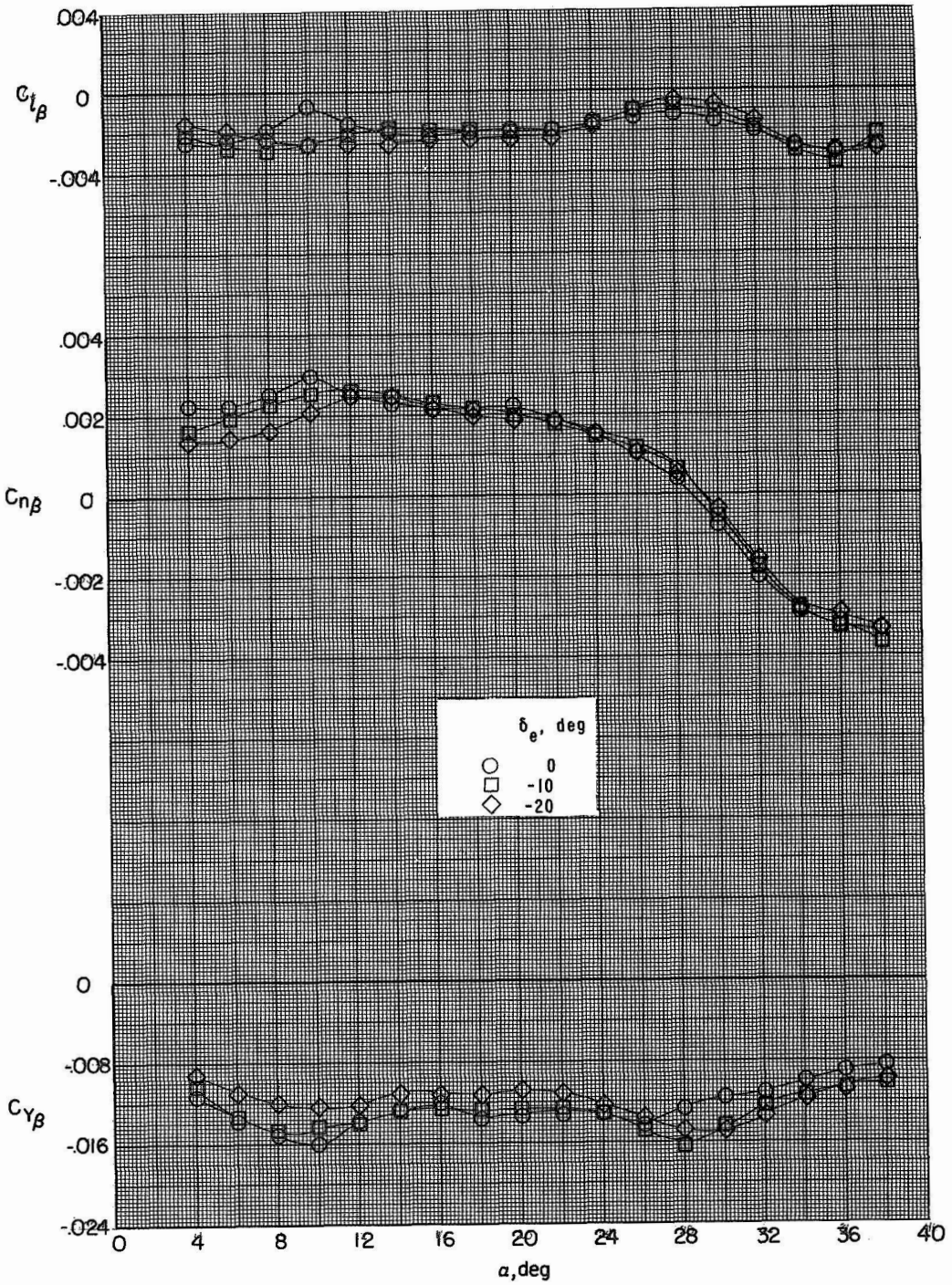

(d) $M = 0.70$; $R_l = 4.7 \times 10^6$.

Figure 5.- Continued.

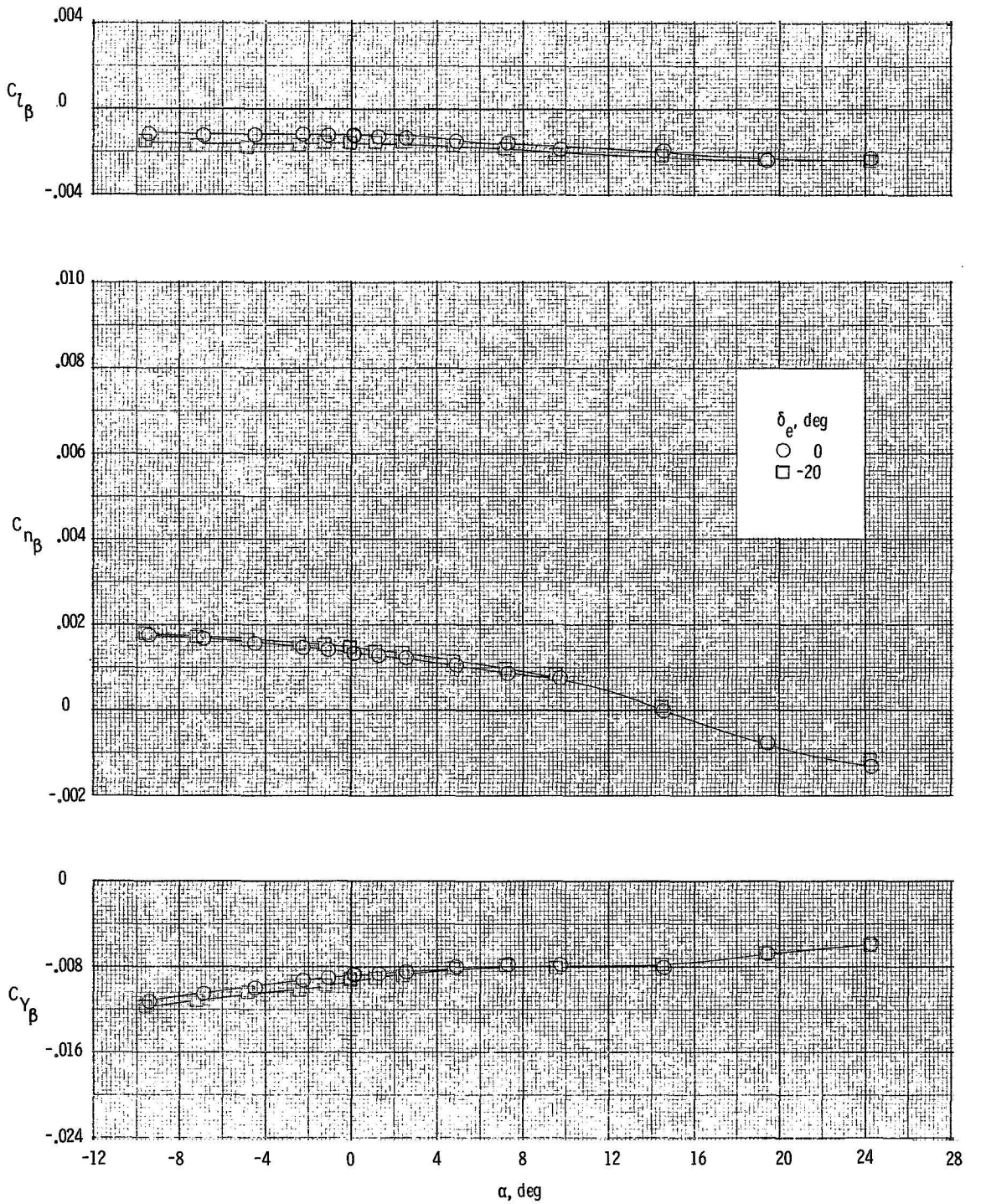

(e) M = 1.50; $R_l = 4.0 \times 10^6$.

Figure 5.- Continued.

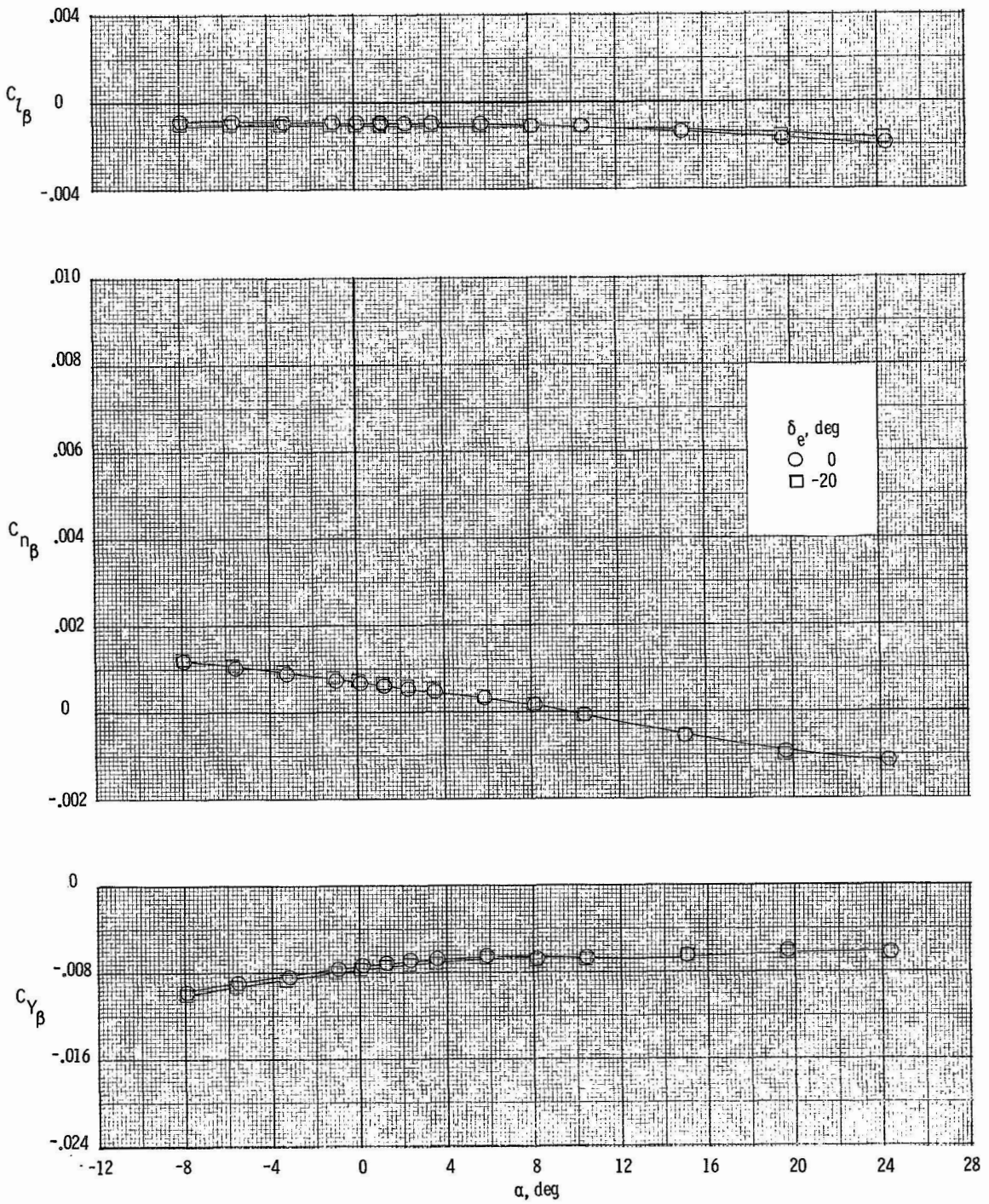

(f) M = 2.16; $R_l = 4.0 \times 10^6$.

Figure 5.- Continued.

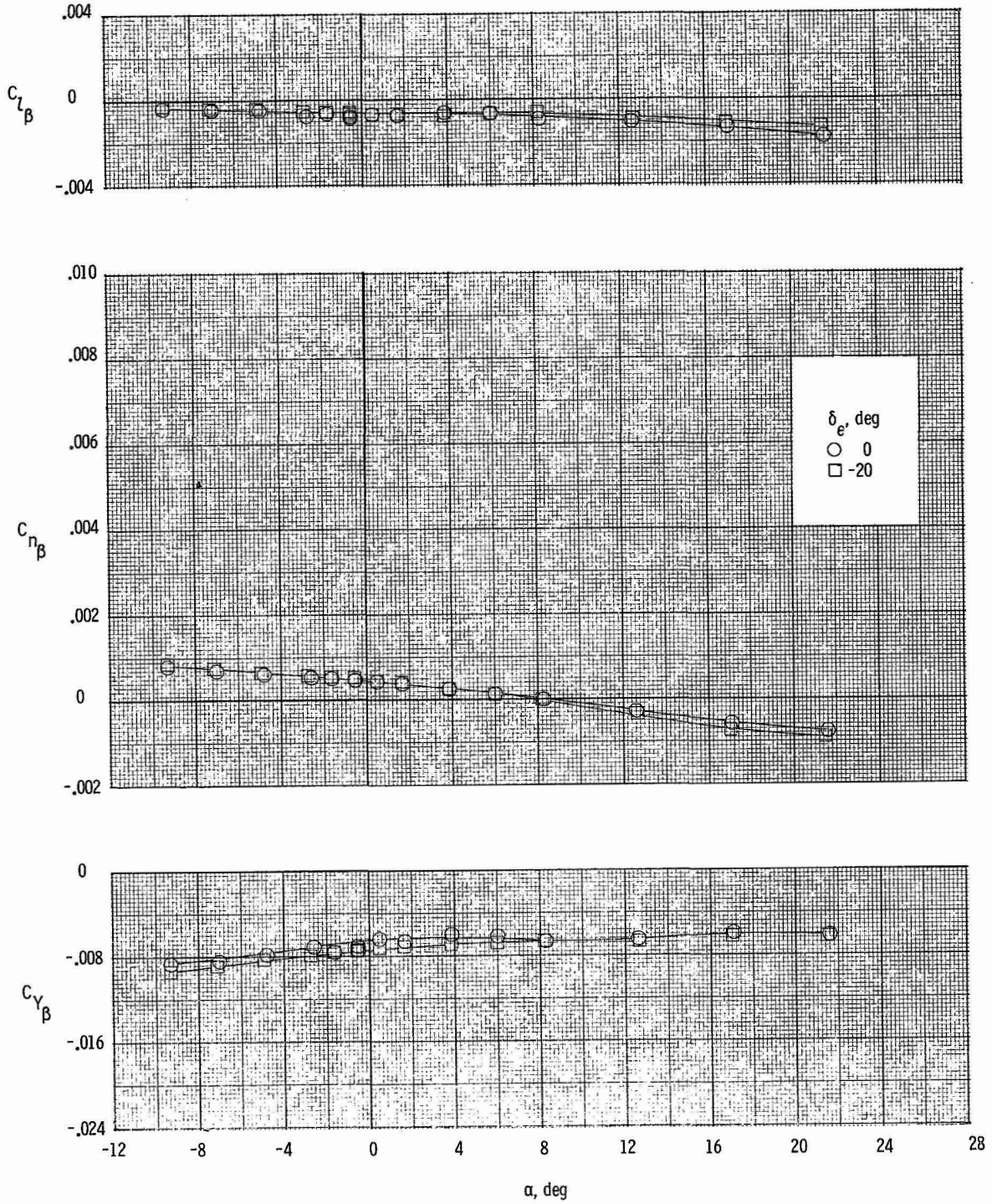

(g) M = 2.86; $R_l = 4.0 \times 10^6$.

Figure 5.- Continued.

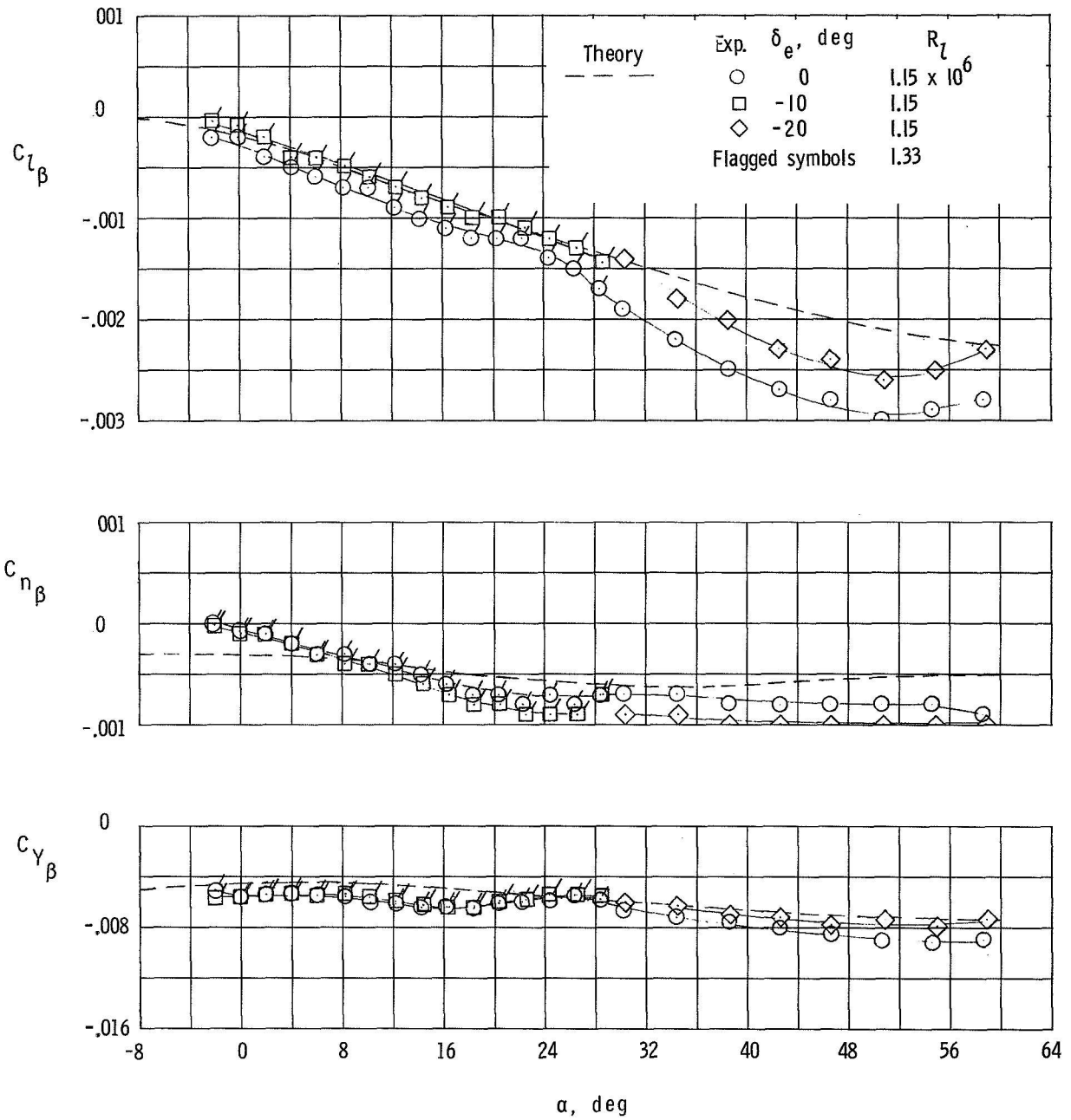

(h) M = 10.4.

Figure 5.- Concluded.

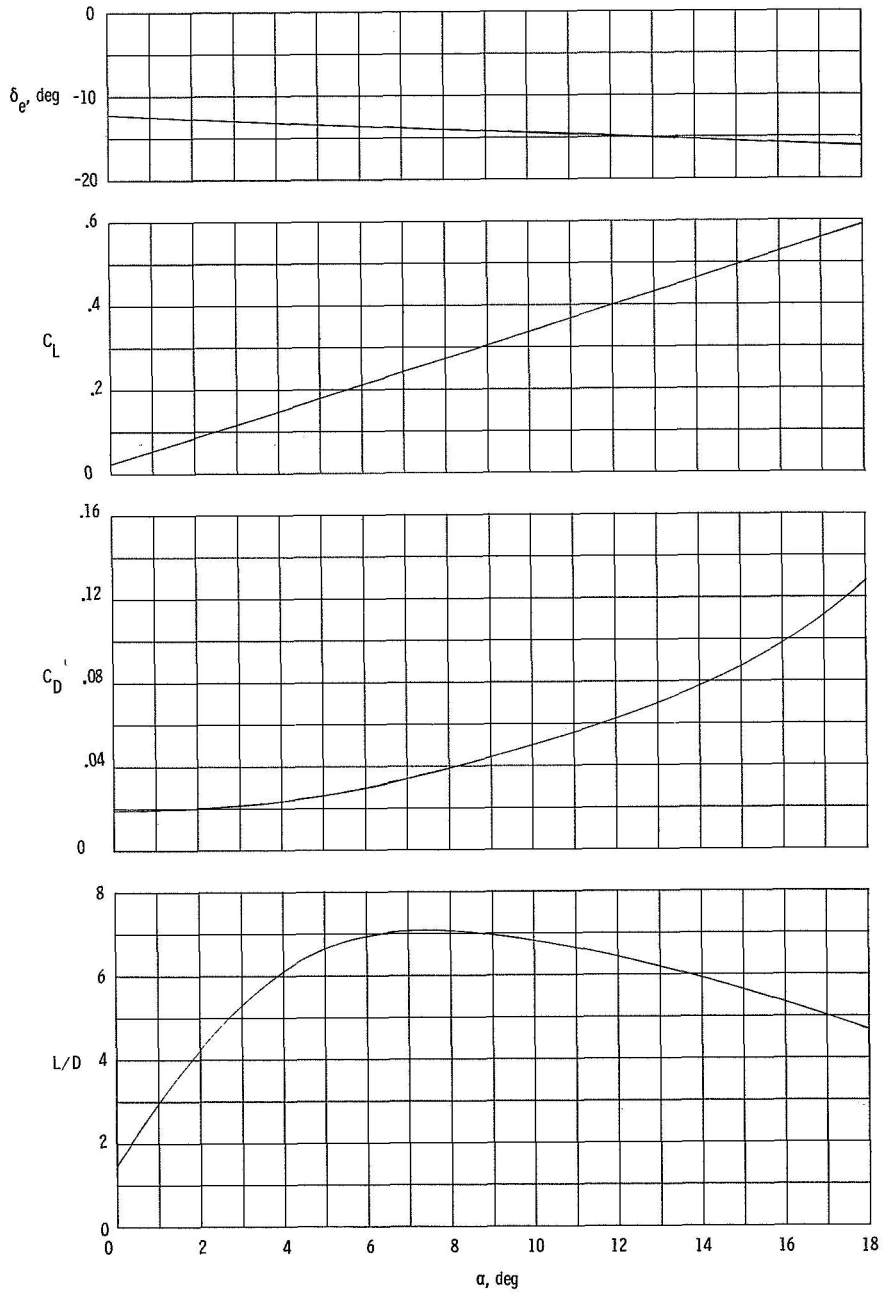

(a) M = 0.28; $R_l = 11.4 \times 10^6$.

Figure 6.- Longitudinal trim characteristics of booster. M = 0.28, 0.60, and 10.4.

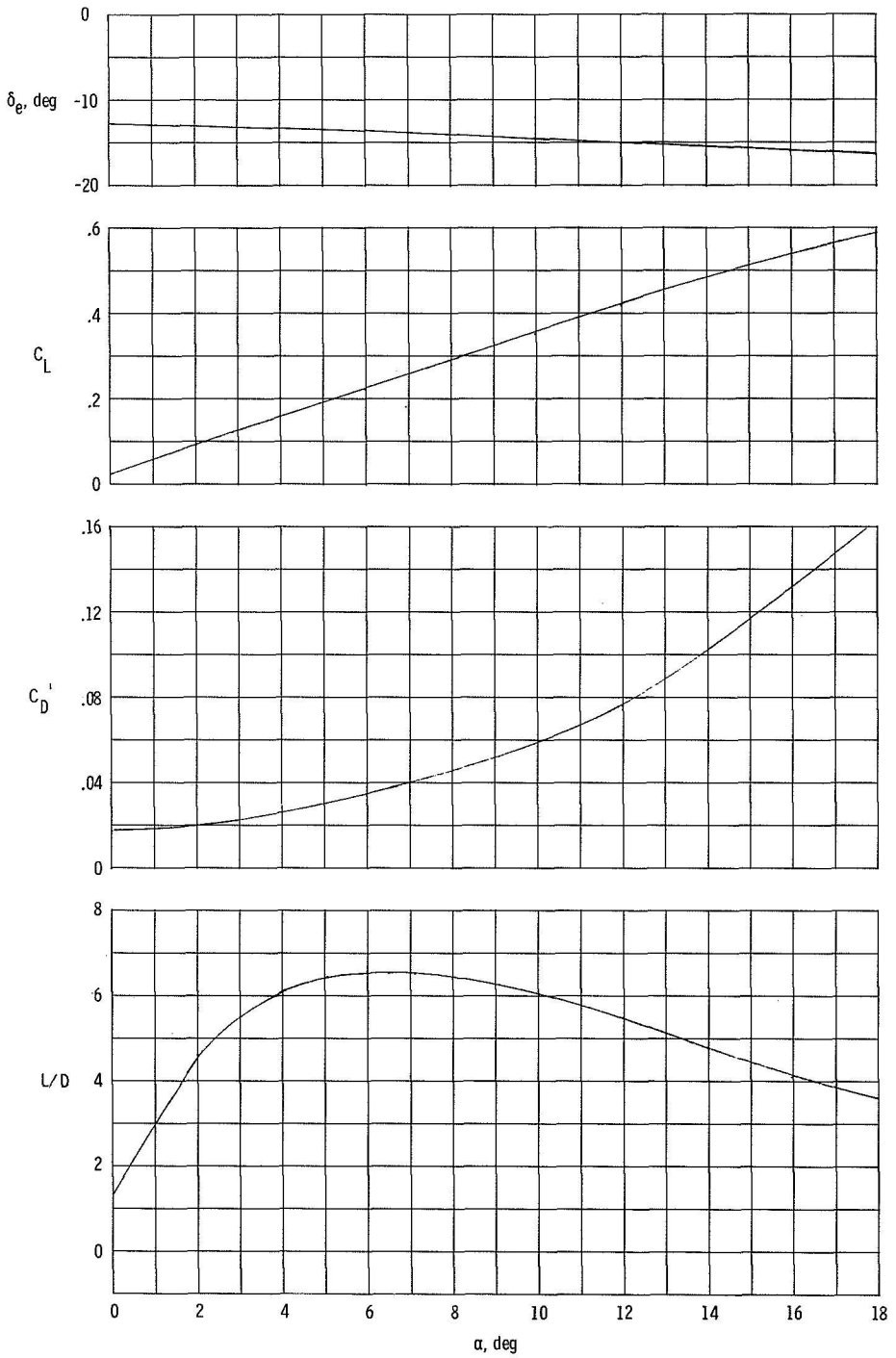

(b) M = 0.60; $R_\ell = 4.5 \times 10^6$.

Figure 6.- Continued.

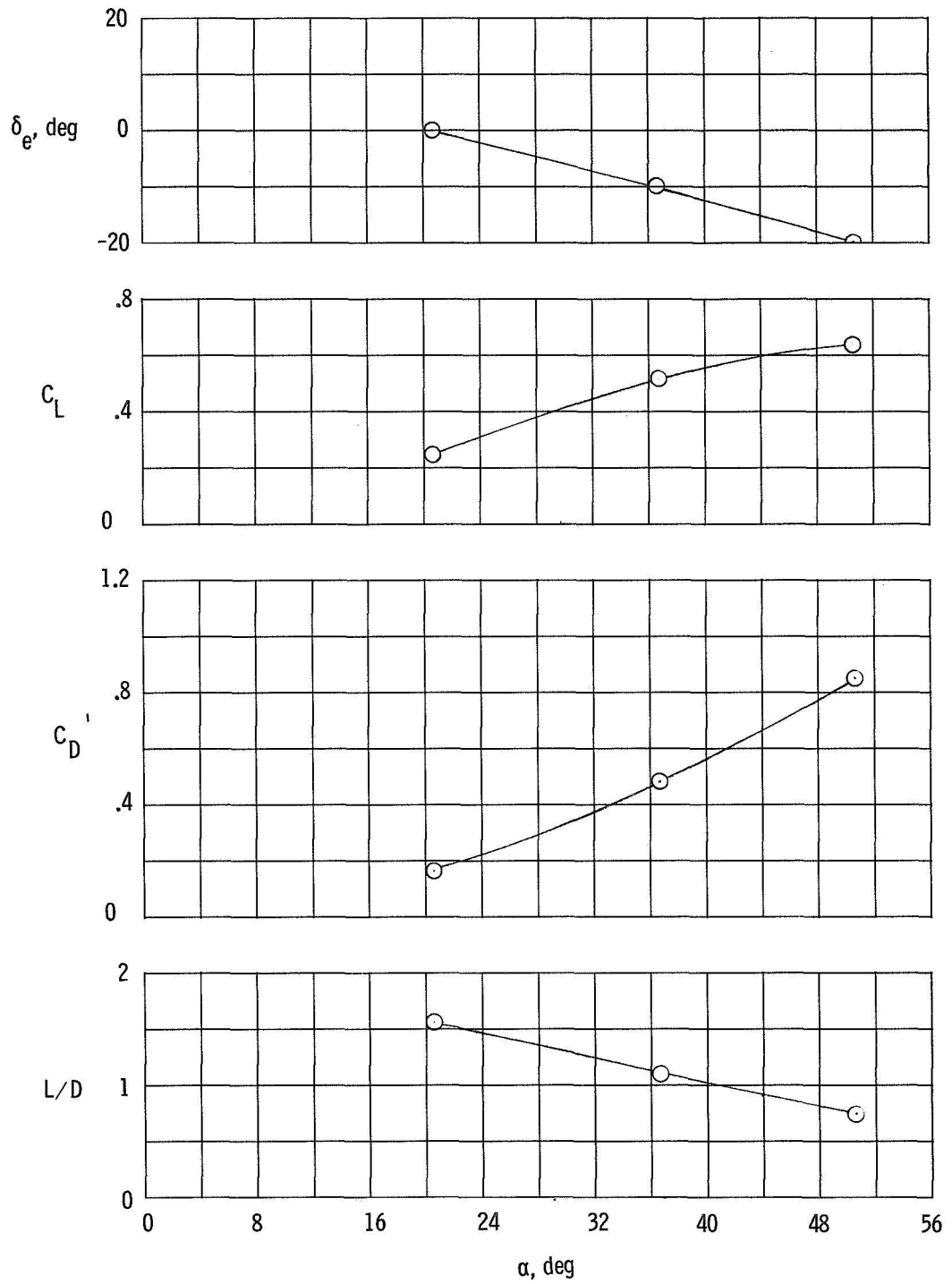

(c) M = 10.4; $R_\ell = 1.33 \times 10^6$ and 1.15×10^6.

Figure 6.- Concluded.

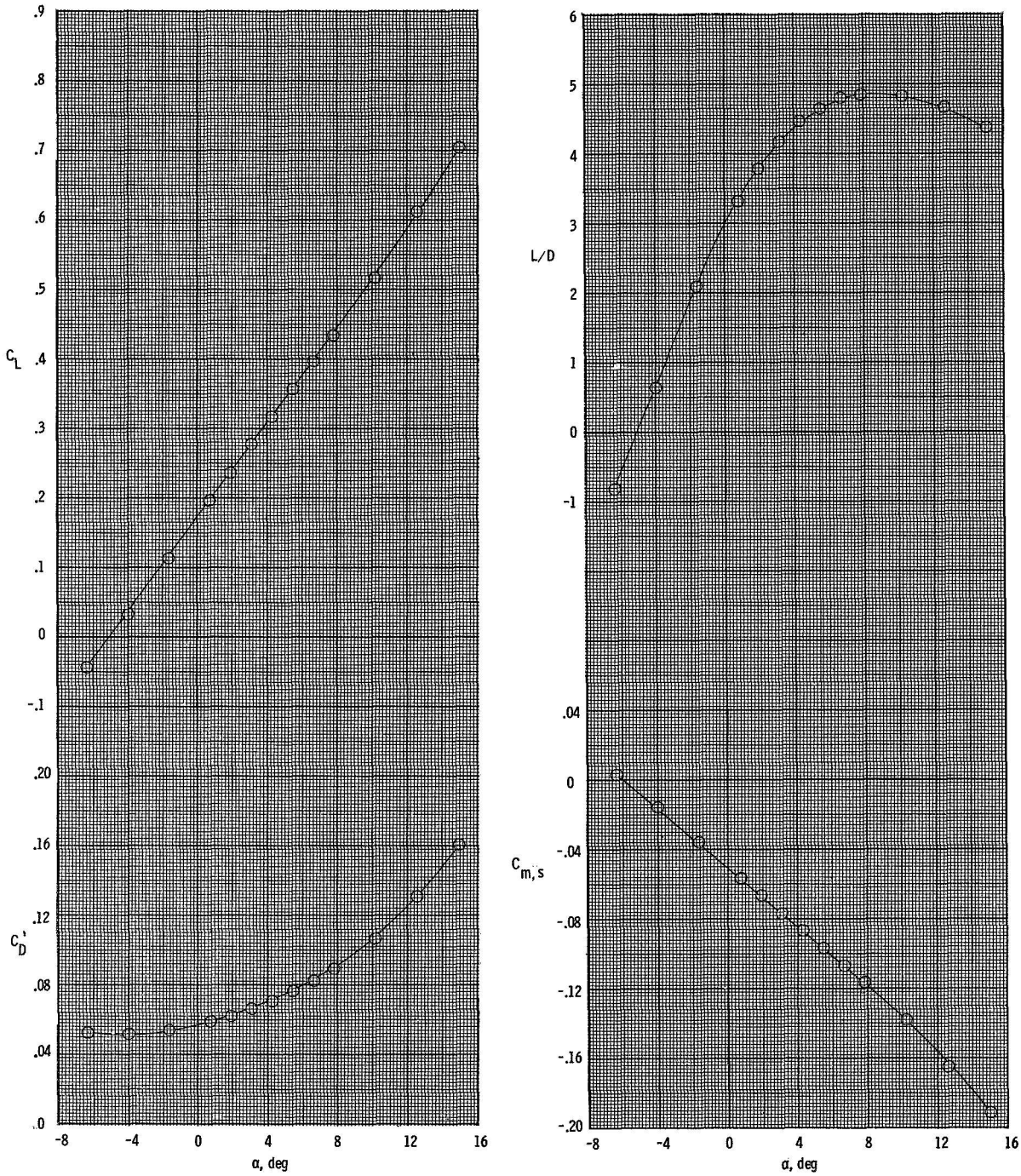

(a) M = 0.28; $R_l = 11.4 \times 10^6$.

Figure 7.- Longitudinal stability characteristics of ascent configuration. $\delta_e = 0^o$; M = 0.28 to 10.4.

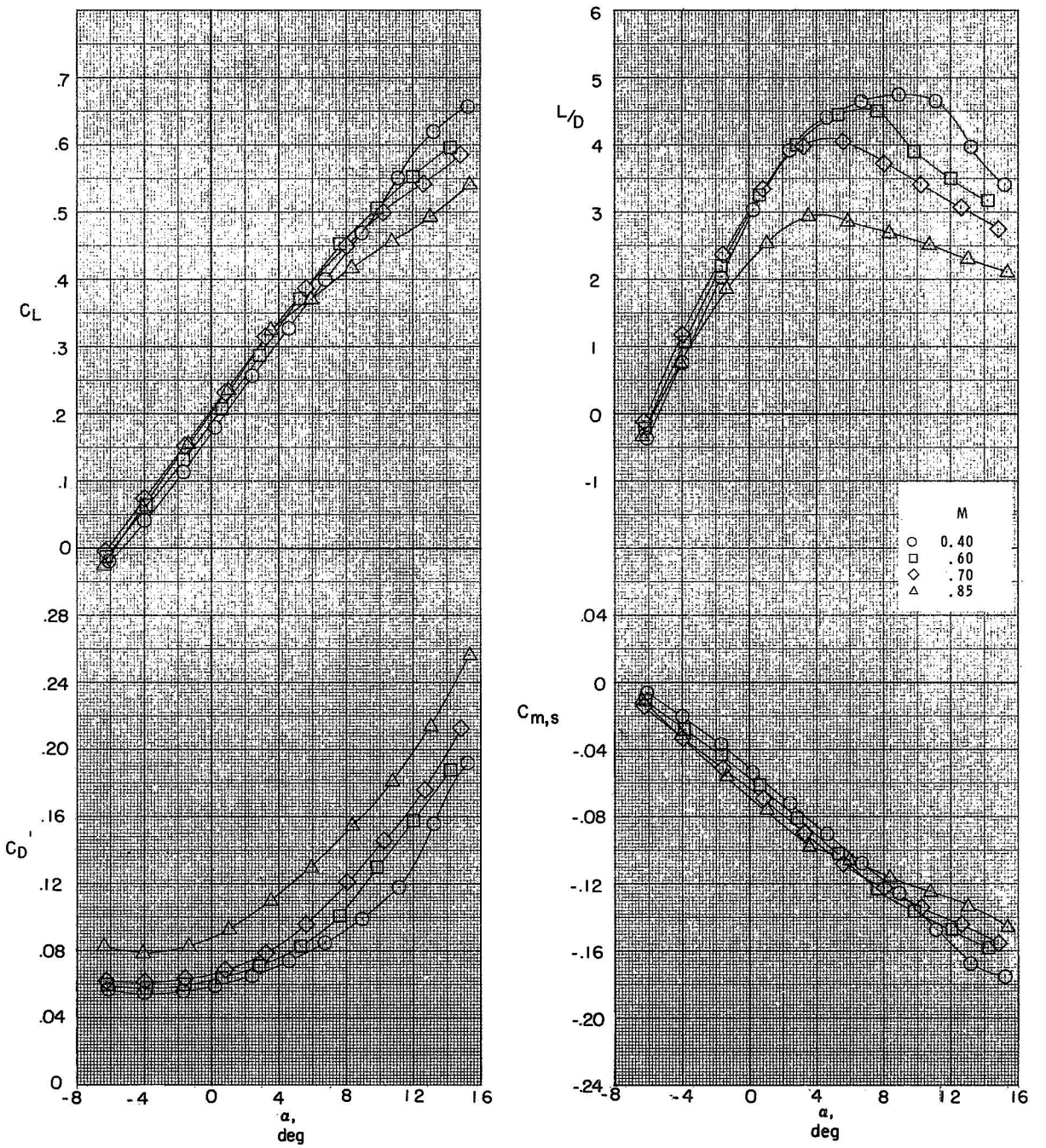

(b) M = 0.40 to 0.85; $R_l = 3.3 \times 10^6$ to 5.2×10^6.

Figure 7.– Continued.

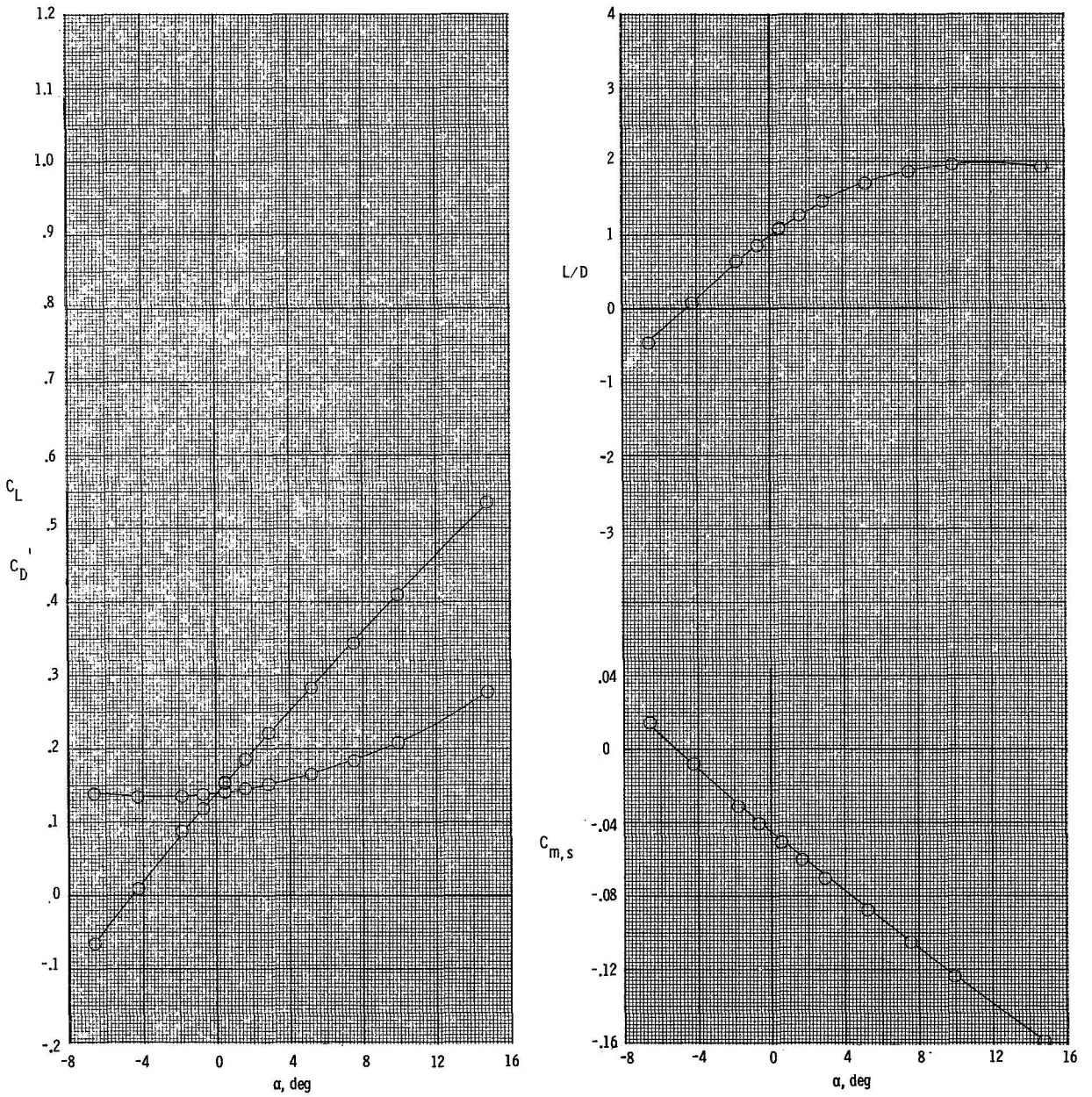

(c) M = 1.50; $R_l = 4.0 \times 10^6$.

Figure 7.- Continued.

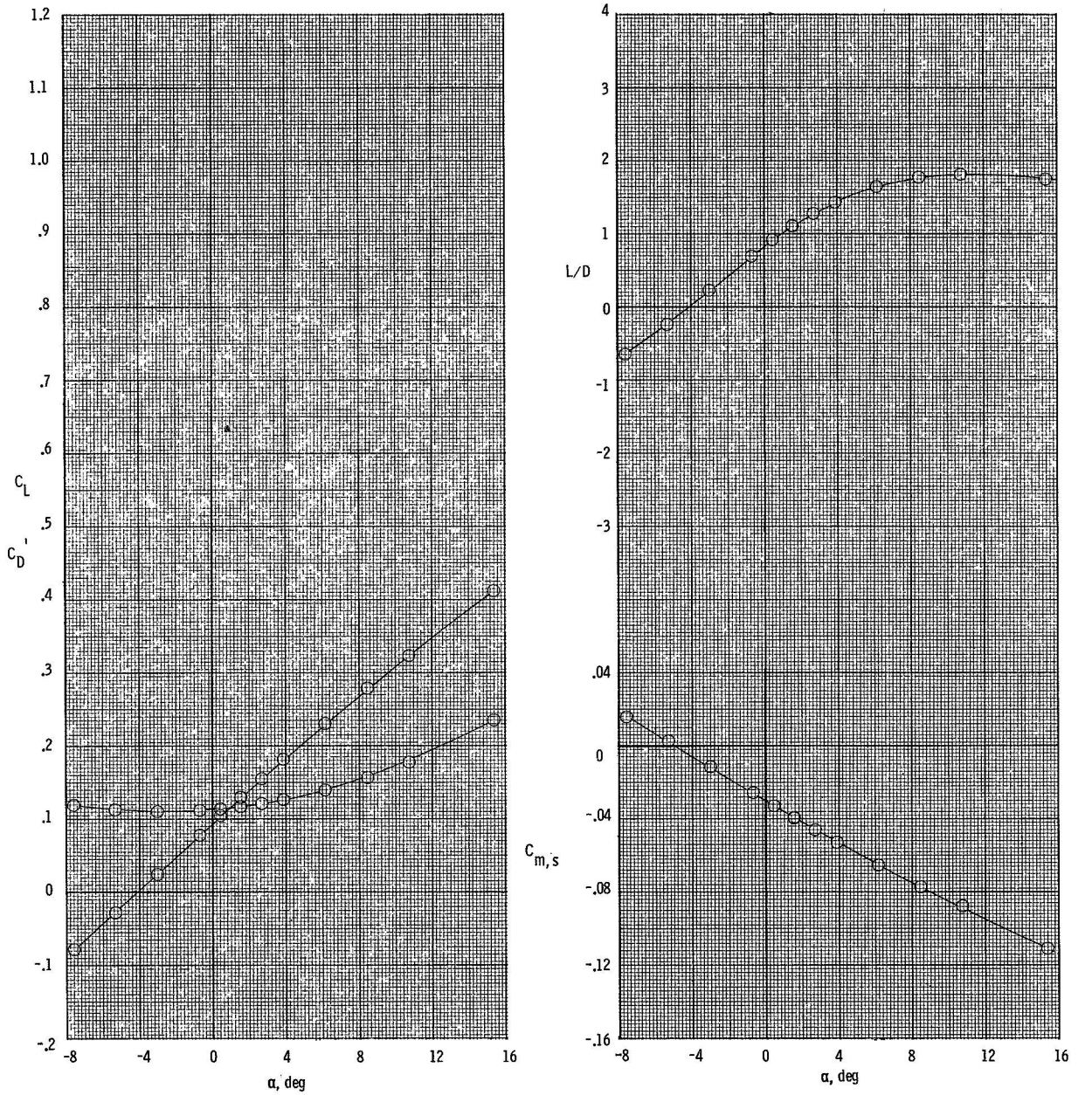

(d) M = 2.16; $R_\ell = 4.0 \times 10^6$.

Figure 7.- Continued.

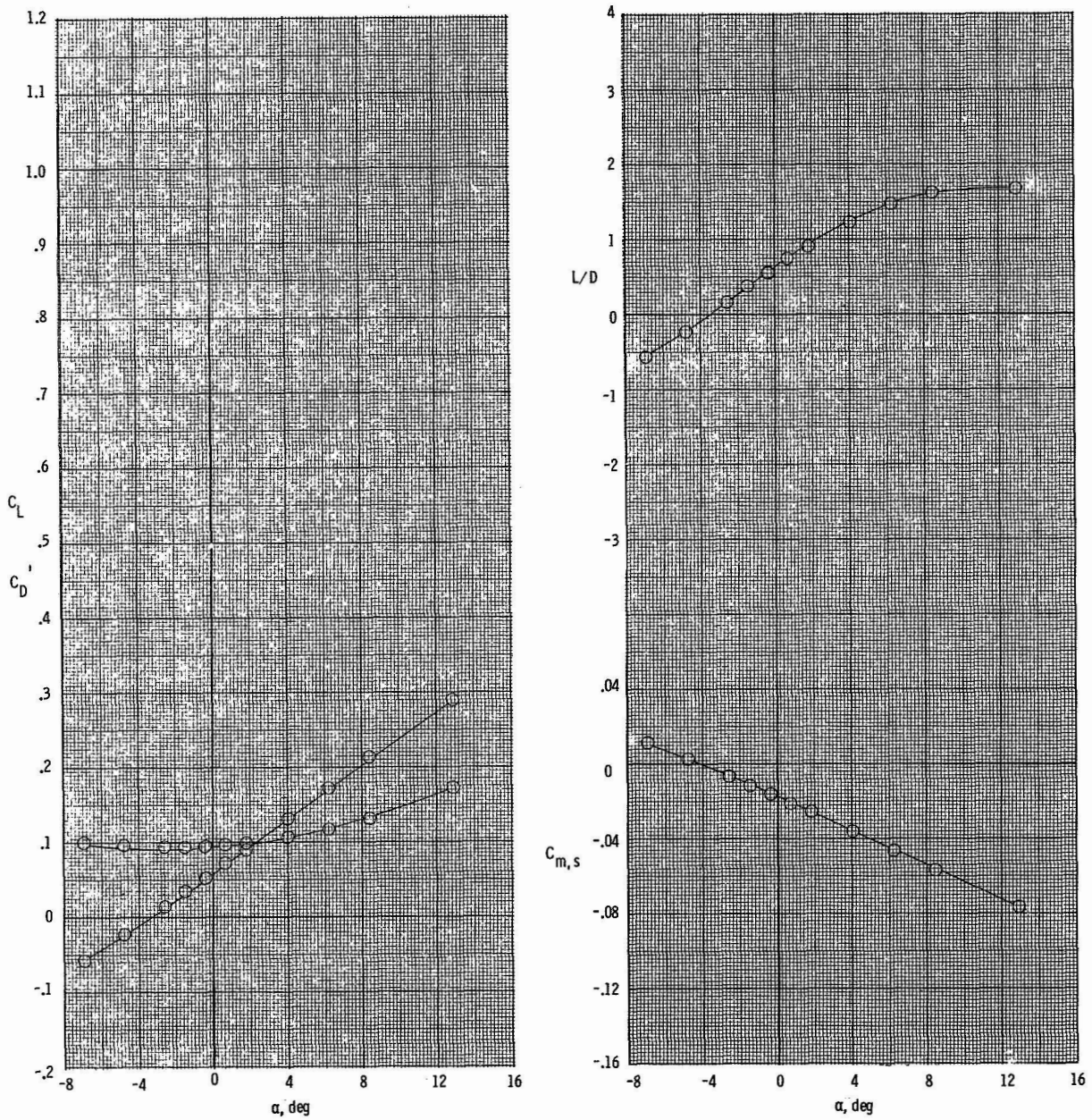

(e) M = 2.86; $R_l = 4.0 \times 10^6$.

Figure 7.- Continued.

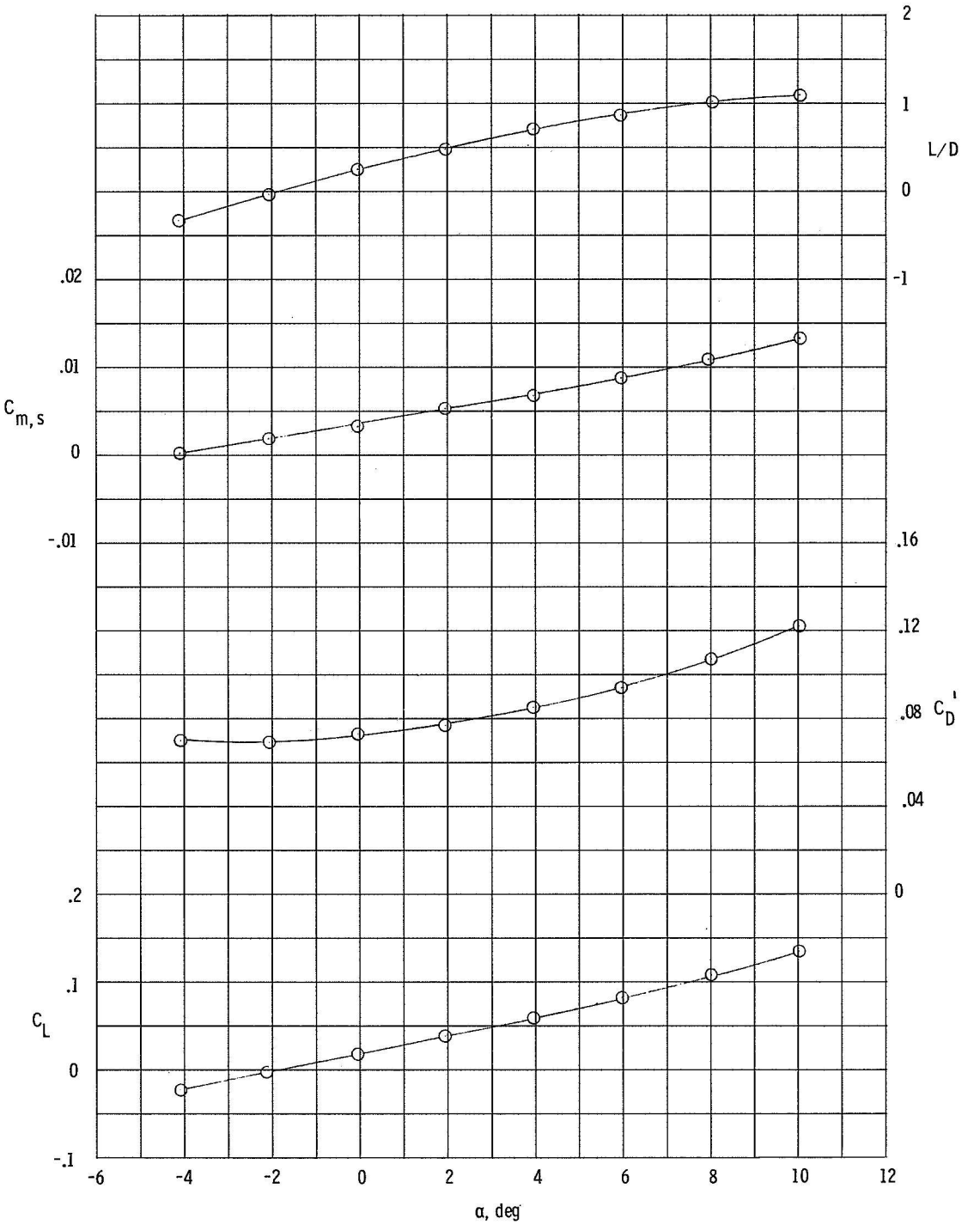

(f) M = 10.4; $R_l = 1.33 \times 10^6$.

Figure 7.- Concluded.

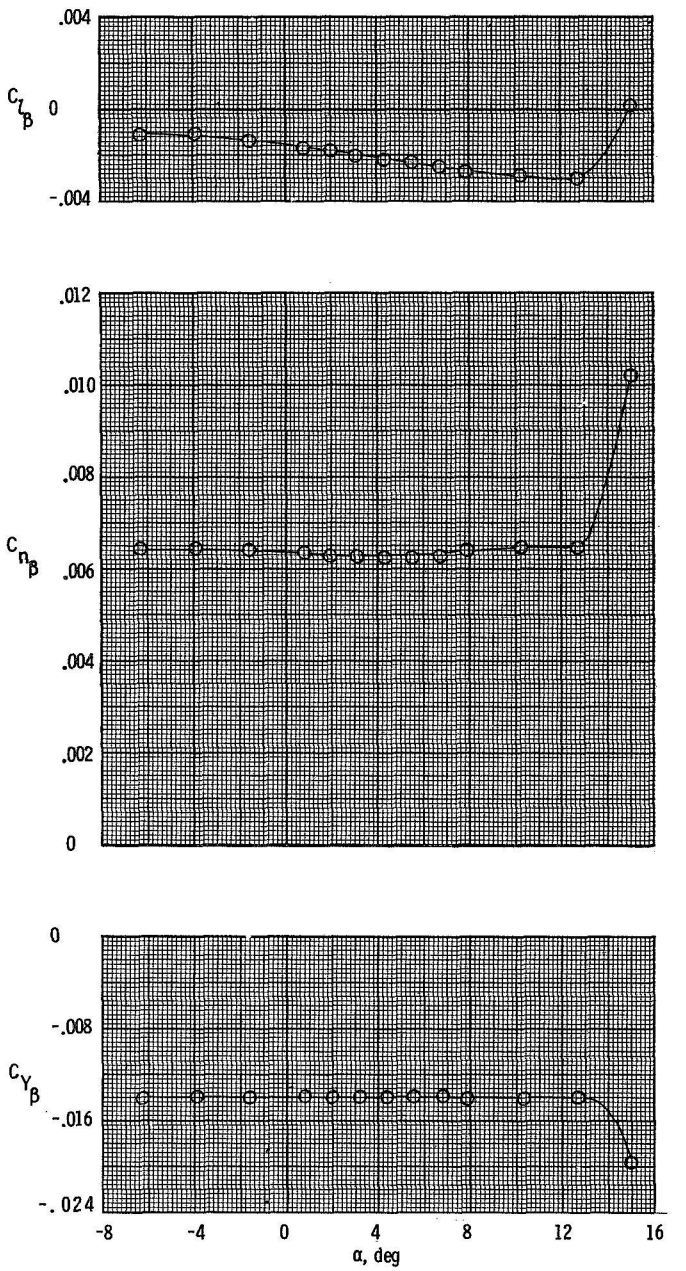

(a) $M = 0.28$; $R_l = 11.4 \times 10^6$.

Figure 8.- Lateral-directional stability characteristics of ascent configuration. $\delta_e = 0^o$; $M = 0.28$ to 2.86.

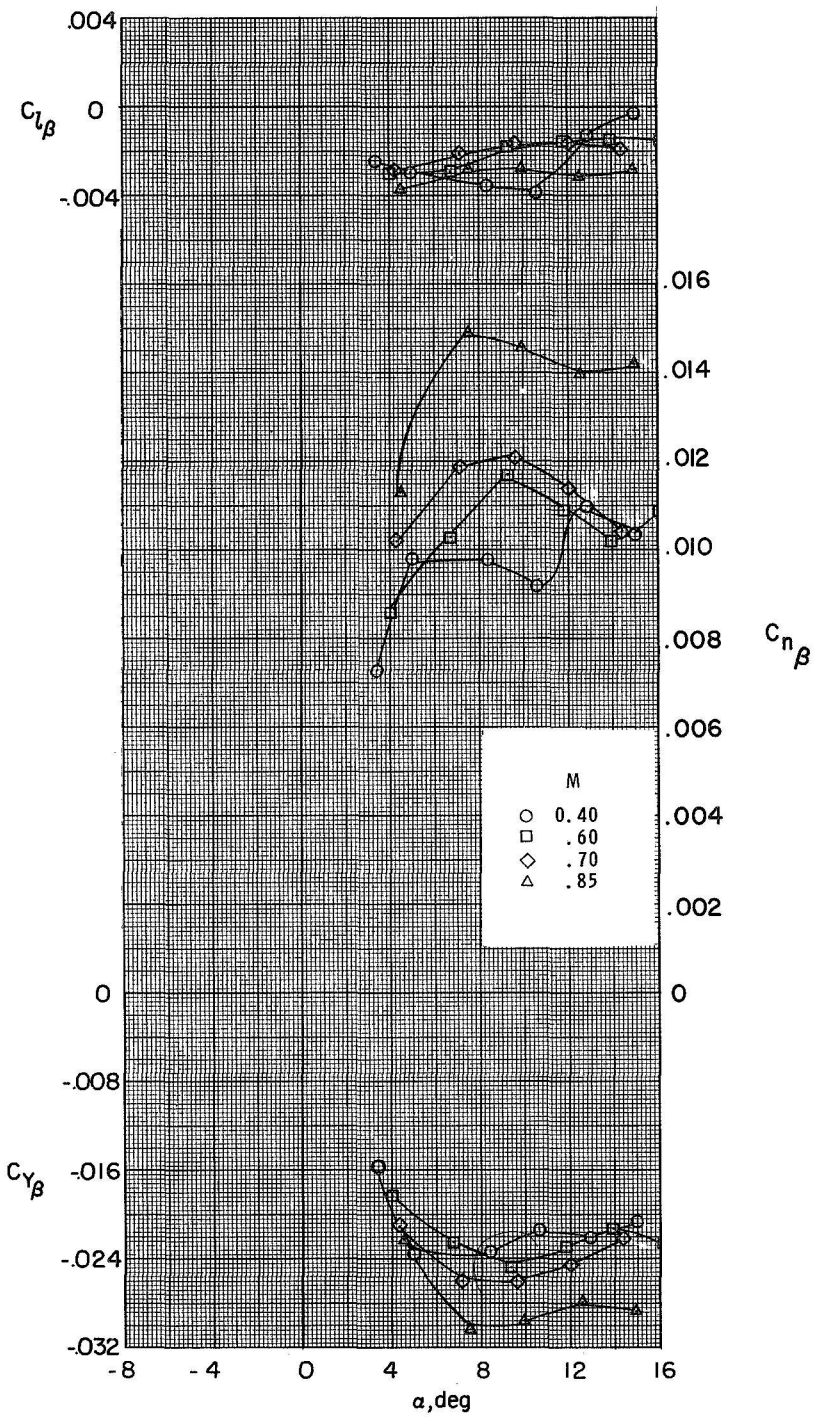

(b) $M = 0.40$ to 0.85; $R_l = 3.3 \times 10^6$ to 5.2×10^6.

Figure 8.- Continued.

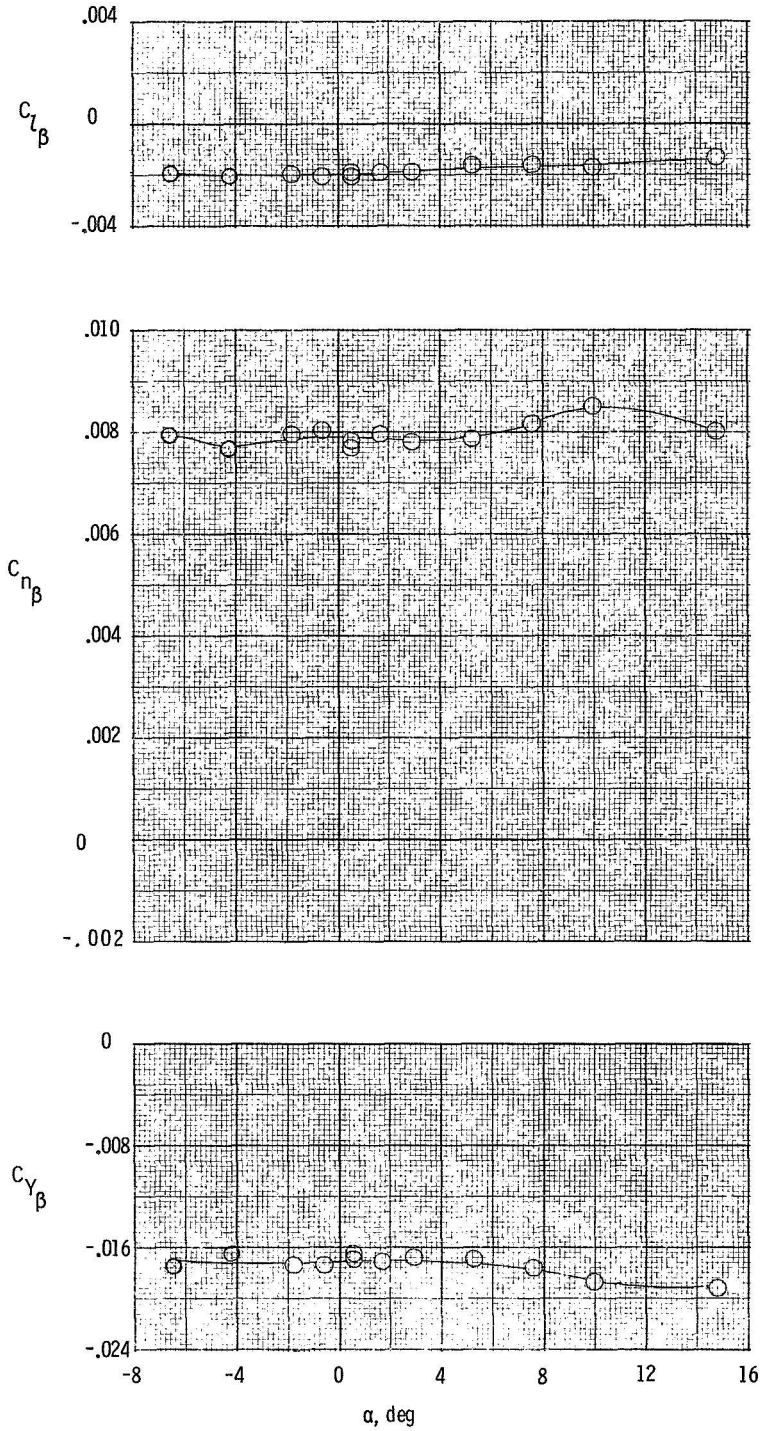

(c) $M = 1.50$; $R_l = 4.0 \times 10^6$.

Figure 8.- Continued.

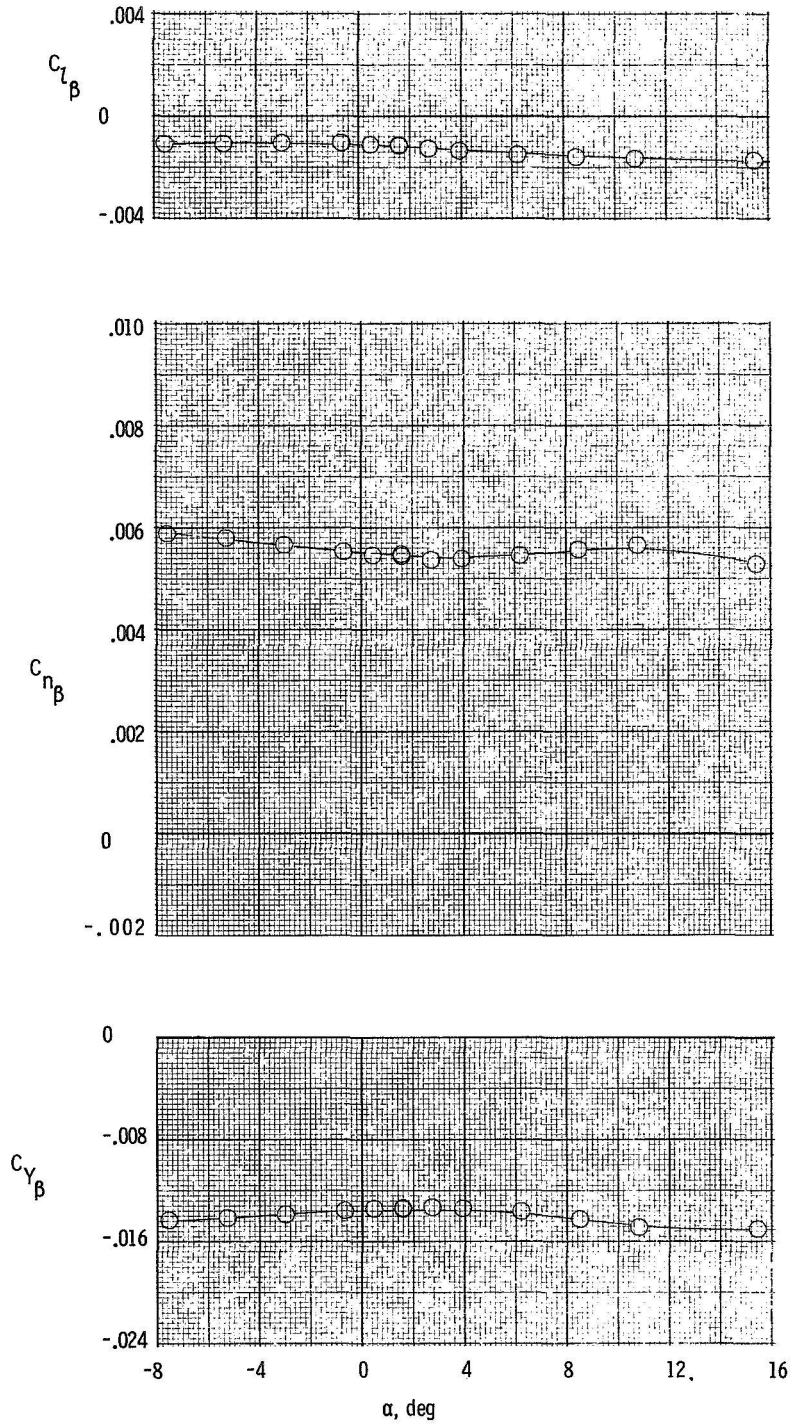

(d) M = 2.16; $R_l = 4.0 \times 10^6$.

Figure 8.- Continued.

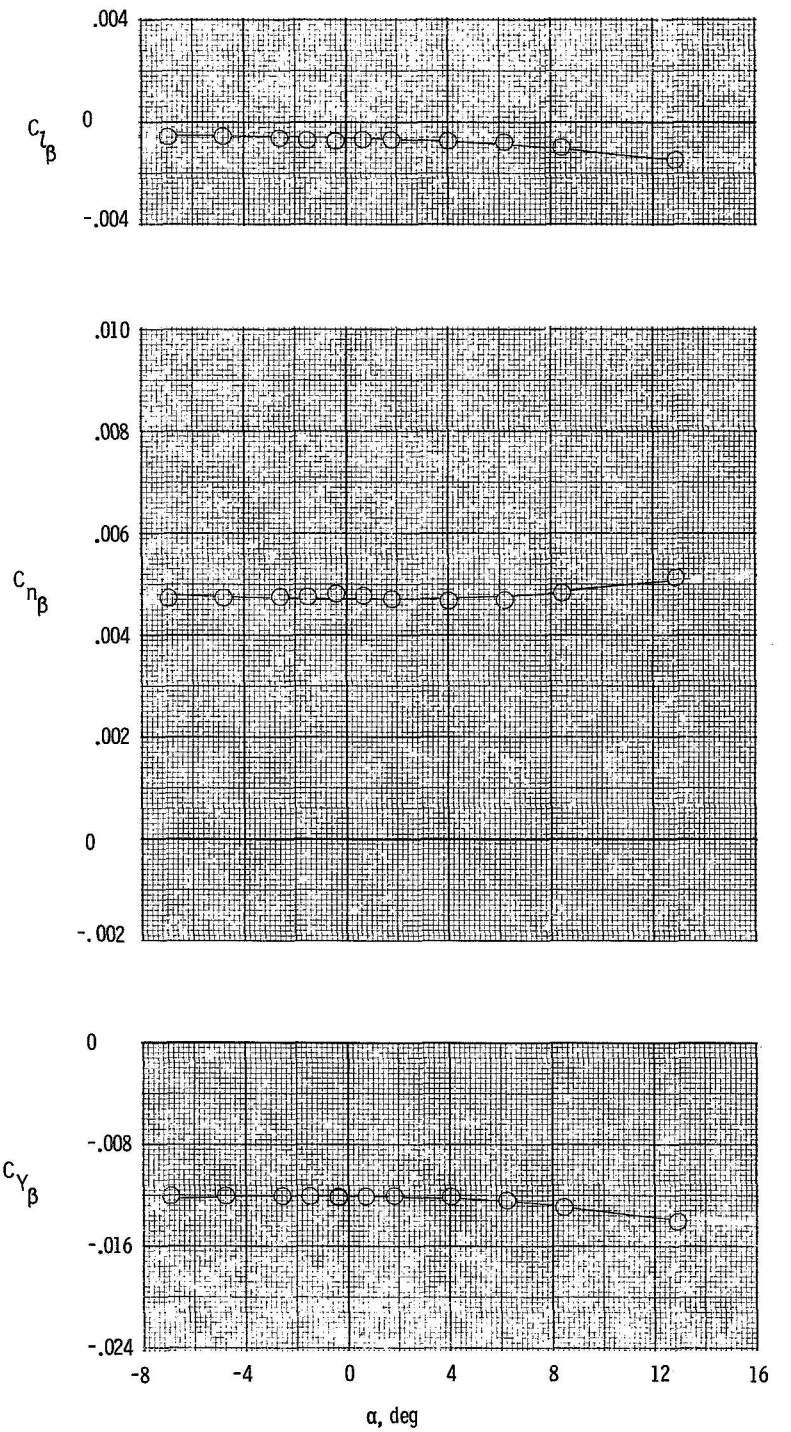

(e) M = 2.86; $R_l = 4.0 \times 10^6$.

Figure 8.- Concluded.

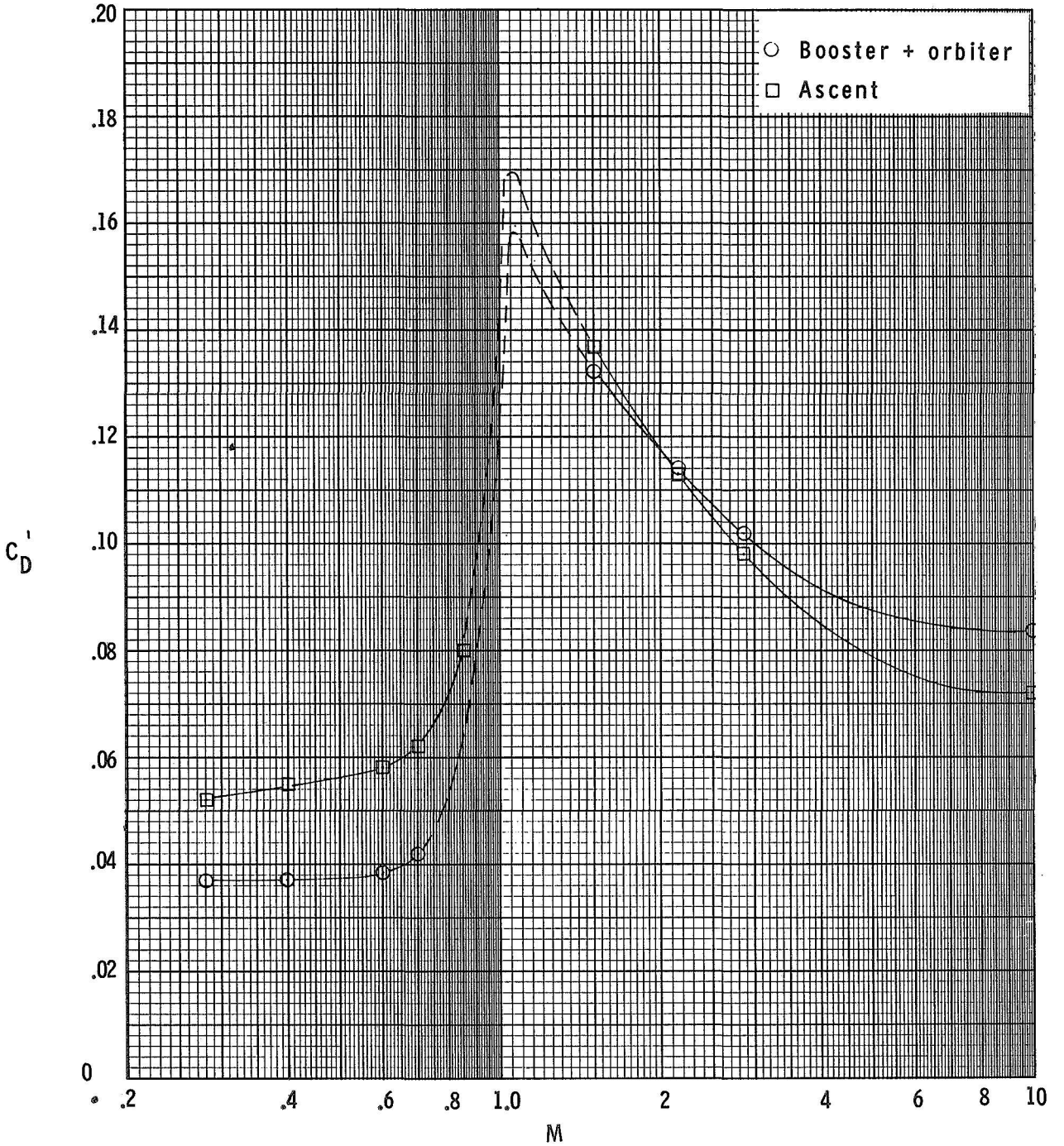

(a) $\alpha = -5^{\circ}$.

Figure 9.- Variation of drag coefficient with Mach number.

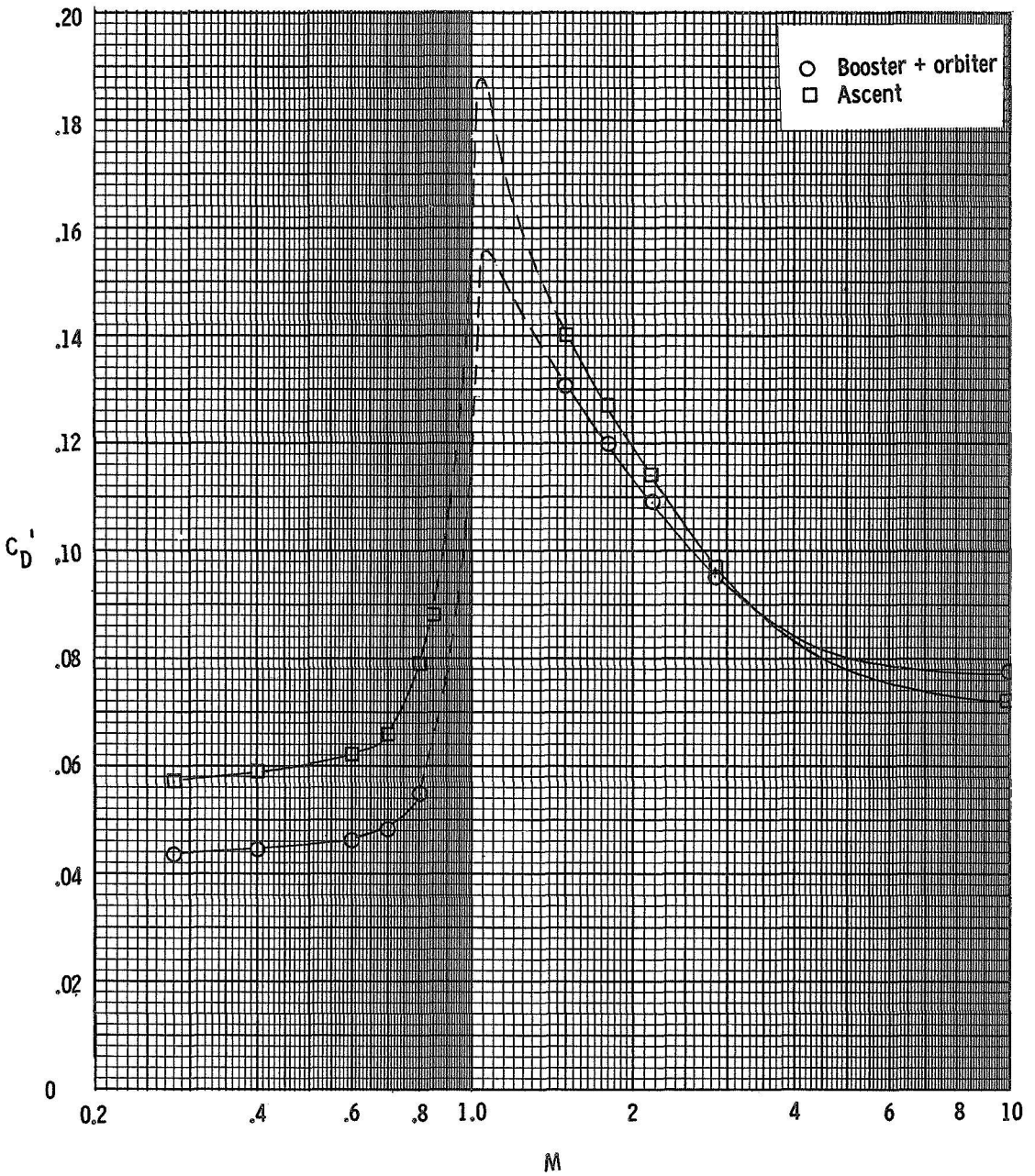

(b) $\alpha = 0^{o}$.

Figure 9.- Continued.

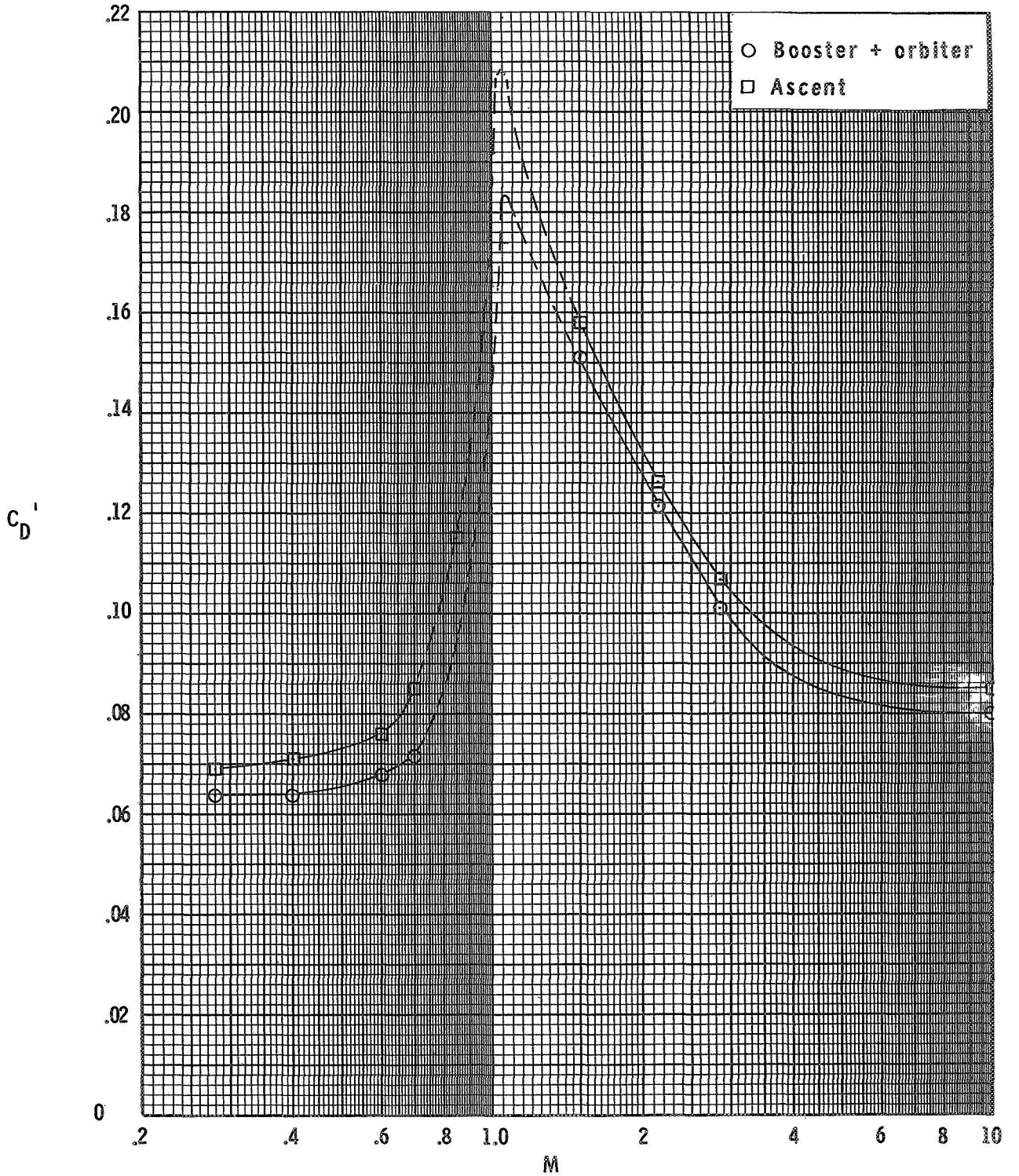

(c) $\alpha = 4^{\circ}$.

Figure 9.- Concluded.

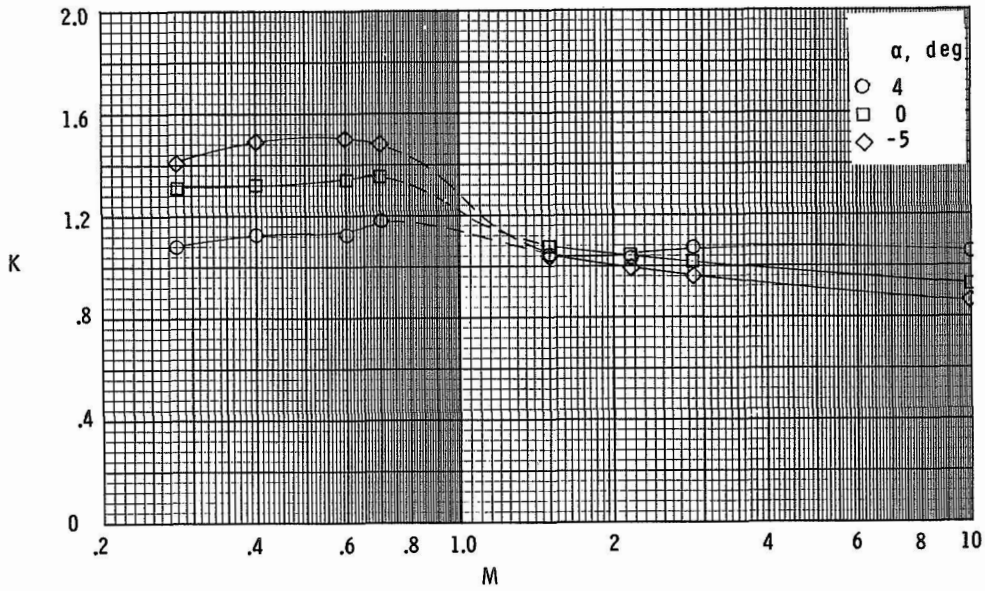

Figure 10.- Variation of interference parameter with Mach number.

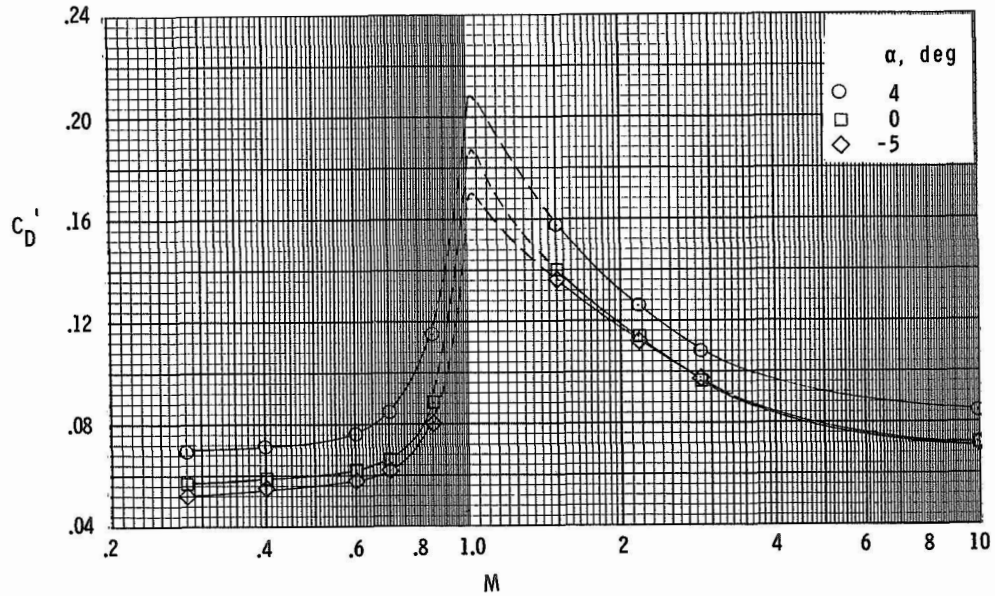

Figure 11.- Drag coefficient of ascent configuration over the Mach number range.

NASA-Langley, 1971 — 31 L-7628

NATIONAL AERONAUTICS AND SPACE ADMINISTRATION
WASHINGTON, D.C. 20546

OFFICIAL BUSINESS
PENALTY FOR PRIVATE USE $300

FIRST CLASS MAIL

POSTAGE AND FEES PAI
NATIONAL AERONAUTICS
SPACE ADMINISTRATION

POSTMASTER: If Undeliverable (Section 1
Postal Manual) Do Not Re

"The aeronautical and space activities of the United States shall be conducted so as to contribute . . . to the expansion of human knowledge of phenomena in the atmosphere and space. The Administration shall provide for the widest practicable and appropriate dissemination of information concerning its activities and the results thereof."

—NATIONAL AERONAUTICS AND SPACE ACT OF 1958

NASA SCIENTIFIC AND TECHNICAL PUBLICATIONS

TECHNICAL REPORTS: Scientific and technical information considered important, complete, and a lasting contribution to existing knowledge.

TECHNICAL NOTES: Information less broad in scope but nevertheless of importance as a contribution to existing knowledge.

TECHNICAL MEMORANDUMS: Information receiving limited distribution because of preliminary data, security classification, or other reasons.

CONTRACTOR REPORTS: Scientific and technical information generated under a NASA contract or grant and considered an important contribution to existing knowledge.

TECHNICAL TRANSLATIONS: Information published in a foreign language considered to merit NASA distribution in English.

SPECIAL PUBLICATIONS: Information derived from or of value to NASA activities. Publications include conference proceedings, monographs, data compilations, handbooks, sourcebooks, and special bibliographies.

TECHNOLOGY UTILIZATION PUBLICATIONS: Information on technology used by NASA that may be of particular interest in commercial and other non-aerospace applications. Publications include Tech Briefs, Technology Utilization Reports and Technology Surveys.

Details on the availability of these publications may be obtained from:

SCIENTIFIC AND TECHNICAL INFORMATION OFFICE

NATIONAL AERONAUTICS AND SPACE ADMINISTRATION

Washington, D.C. 20546